The Faculty of Engineering,
Science and Medicine
Department of Health Science and Technology
Fredrik Bajers Vej 7D, DK-9220 Aalborg Øst
Telefon + 45 96 35 80 80
Fax + 45 98 15 40 08
http://www.hst.aau.dk

Title:

Use of current source density analysis to characterize subthalamic nucleus response following deep brain stimulation

Theme:

Applied biomedical engineering and informatics

Project period:

Spring semester 2010

Project group:

ST 1085d

Group members:

Majken Munch

Supervisor:

Winnie Jensen

Number of copies: 3

Number of pages: 59

Finished 17th of June, 2010

Abstract:

Parkinson's disease is a neurological disorder, whose classical symptoms are tremor, rigidity and slowness of movement. These symptoms are caused by degeneration of dopamine-producing neurons in the substantia nigra. High frequency deep brain stimulation (DBS) to the subthalamic nucleus has been found to improve the symptoms. The purpose of DBS is to generate extracellular electric fields which can modify pathological neural activity in the basal ganglia. Many theories have been proposed to explain how this modification takes place, but no clear answer has yet been found.

Local field potentials (LFP) can give information about the functionality of the neural networks of the brain, and using current source density (CSD) analysis on LFP signals can provide more information on local spatial relations, than the LFP signals alone. The main hypothesis of this project is that CSD analysis can be used to characterize and quantify changes in the neural network following DBS.

Data were gathered at University of Lübeck, Germany, from rat experiments where LFP signals were recorded in the subthalamic nucleus before and after DBS. Two different types of experiments were performed: one that varied the duration of stimulation and one that varied the amplitude. The data were subsequently analysed using CSD analysis, and features were extracted and used to compare the activity before and after stimulation. The features were RMS values of CSD signals at each depth, the number of times the CSD signals crossed a predetermined threshold, and the intervals between the threshold crossings.

The results showed that the RMS values of the CSD signals most often decreased after DBS. The number of threshold crossings also changed following DBS but a specific pattern was less clear. The intervals between threshold crossings showed no clear changes following DBS.

AALBORG UNIVERSITET

Det Ingeniør-, Natur- og Sundheds-videnskabelige Fakultet
Institut for Sundhedsvidenskab og Teknologi
Fredrik Bajers Vej 7D, DK-9220 Aalborg Øst
Telefon + 45 96 35 80 80
Fax + 45 98 15 40 08
http://www.hst.aau.dk

Titel:

Brug af current source density analyse til at karakterisere response fra nucleus subthalamicus efter deep brain stimulation

Tema:

Anvendt sundhedsteknologi og informatik

Projektperiode:

Forårssemesteret 2010

Projektgruppe:

ST 1085d

Gruppemedlemmer:

Majken Munch

Vejleder:

Winnie Jensen

Oplagstal: 3

Sidetal: 59

Afsluttet den 17. juni, 2010

Synopsis:

Parkinsons sygdom er en neurologisk sygdom, hvis klassiske symptomer er rystelser, stivhed og langsomme bevægelser. Symptomerne skyldes degeneration af dopamin-producerende neuroner i substantia nigra. Højfrekvent deep brain stimulation (DBS) i nucleus subthalamicus har vist sig at kunne forbedre symptomerne. Formålet med DBS er at generere ekstra-cellulære elektriske felter, der kan modificere patologisk neural aktivitet i basalganglierne. Mange teorier om hvordan denne modification fungerer er blevet foreslået, men der er endnu ikke blevet fundet et klart svar.
Local field potentials (LFP) kan give information om funktionaliteten af the neurale netværk i hjernen, og brugen af current source density (CSD) analyse på LFP signalerne kan give mere information om lokale spatiale relations end LFP signalerne alene kan. Hovedhypotesen for dette projet er at CSD analyse kan bruges til at karakterisere og kvantifisere ændringer i det neurale netværk efter DBS.
Data blev indsamlet ved Lübeck Universitet i Tyskland fra rotte-eksperimenter hvor LFP signaler blev optaget i nucleus subthalamicus før og efter DBS. To forskellige eksperimenter blev udført: et hvor længden af stimulation blev varieret og et hvor amplituden blev varieret. Data blev bagefter analyseret ved hjælp af CSD analyse og features blev udtrukket og brugt til at sammenligne aktiviteten før og efter stimulation. Featurene var RMS værdier af CSD signalerne for hver dybde, det antal gange CSD signalerne krydsede en given tærskelværdi og tidsintervallerne mellem tærskelværdi-krydsningerne.
Resultaterne viste at RMS værdierne af CSD signalerne oftest faldt efter DBS. Antallet af tærskelværdi-krydsninger ændredes også efter DBS, men der var ikke et tydeligt mønster. Intervallerne mellem tærskelværdi-krydsninger viste ingen klare ændringer efter DBS.

Preface

This report was written during the fourth semester of the Master of Science in Engineering (M.Sc.E) program in Biomedical Engineering and Informatics (BMEI) at the department of Health Science and Technology at Aalborg University, Denmark.

To gather data for the project, I visited Institute for Signal Processing, University of Lübeck, in Germany, from February 14th to March 14th 2010, where experiments were carried out in collaboration with Department for Neurology, University of Lübeck.

The experiments used in the project were carried out on Februray 2nd and March 19th 2010, at University of Lübeck.

I wish to thank Susanne Löffler, Department for Neurology, University of Lübeck, for carrying out the experiments and sharing the data, and Ulrich G. Hoffman, Institute for Signal Processing, University of Lübeck, for support with interpreting the data.

Aalborg University, June 2010

Majken Munch

Table of contents

Chapter 1

Introduction

Parkinson's disease (PD) is a degenerative neurological disorder. It is most often diagnosed between the ages of 50 and 60 years, and it becomes more frequent with increased age. It has an estimated prevalence of 1 per 1,000 inhabitants in Denmark (Parkinsonforeningen, 2010)

The classical symptoms of PD are tremor, rigidity and slowness of movement, and these symptoms are caused by degeneration of dopamine-producing neurons in a part of the brain called the substantia nigra. It is not yet known what causes the neuronal degeneration (Jankovic, 2008; Lees et al., 2009).

The primary treatment for PD is a drug called Levodopa, which is converted to dopamine after it has passed the blood brain barrier. Levodopa generally improves the symptoms for many years, but very often side effects such as involuntary movements increase in intensity (Olanow et al., 2009).

High frequency deep brain stimulation (DBS) to an area of the brain called the subthalamic nucleus has been found to improve symptoms, and lessen the debilitating side effects that can occur after long periods of Levodopa use (Olanow et al., 2009). Implantation of deep brain stimulators has therefore become a treatment option for many PD patients (Factor and Weiner, 2007a)

The purpose of DBS is to generate extracellular electric fields in the brain tissue, which can modify pathological neural activity. The fields generate voltage distributions along the neural processes, and in turn the voltage distributions generate transmembrane current flow (McIntyre, 2009).

Many different theories have been proposed to explain how DBS works to change the neural activity, but no clear answer has been found yet. It is therefore necessary to adjust stimulation parameters for each patient until symptoms show improvement (McIntyre, 2009).

Investigation of brain signals in relation to DBS may provide information, which can be used to determine which of the many theories best describe how DBS works, and to design more optimal stimulation strategies.

There are many ways of investigating brain activity. However, narrowing the question to electrophysiological methods, reveals to major areas: the investigation of local field poten-

tials (LFP) and the investigation of spikes (i.e. single unit action potentials). LFP gives information about the network function, whereas spikes only give information about individual neurons (Logothetis, 2008). Using current source density (CSD) analysis on LFP signals can provide more information on local spatial relations, than the LFP signals alone, and it is therefore interesting to use CSD analysis to investigate network function in relation to DBS (Mitzdorf, 1985). Thus, the main hypothesis of the project is:

1.1 Problem statement

CSD analysis can be used to characterize and quantify changes in the functioning of the neural network following DBS.

1.2 Solution strategy

In order to investigate the hypothesis, two major steps were needed:

1: Data were gathered from rat experiments, where LFPs were recorded with a linear electrode array placed in the subthalamic nucleus. Recordings were made before and after deep brain stimulation provided by a stimulation electrode on the same electrode array. Two different types of experiments were performed: One, in which the stimulus amplitude was fixed and the duration of stimulation was varied, and another, in which the stimulation duration was fixed and the amplitude varied.

2: Data were analysed using CSD analysis. The report presents the results of comparing RMS values of the CSD signals before and after stimulation, the results of comparing how often the CSD signals crosses a predetermined threshold, and the results of comparing how long intervals between threshold crossings are.

1.3 Limitations

- The experiments were only performed on one rat each.
- The rats were healthy rats, not Parkinson models, which means that the project cannot investigate the effect of DBS on pathological networks.
- LFPs could not be recorded during the stimulation due to large stimulation artefacts.
- There are no external triggers, with which the LFPs can be synchronised, so the CSD analysis is performed on spontaneous data

Chapter 2

Anatomy and physiology of the basal ganglia

In order to understand the effects of deep brain stimulation, it is necessary first to understand the basal ganglia, which both the substantia nigra and the subthalamic nucleus are part of. This chapter begins with a description of the anatomy of the basal ganglia, followed by a description of the main motor-related pathways through the basal ganglia.

The basal ganglia consist of groups of neuron cell bodies located deep in the brain, lying around the lateral ventricle in each hemisphere, see figure 2.1. The basal ganglia are surrounded by myelinated axons, that carry information between different parts of the brain. (Martini, 2006)

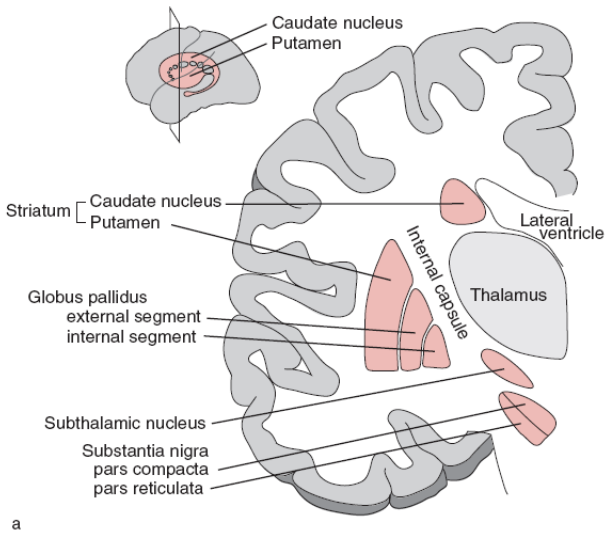

Figure 2.1: The location of the basal ganglia components (Nambu, 2009)

Although the basal ganglia have been studied for many years, their primary function is still not fully known (Nambu, 2009). The long-held hypothesis that the basal ganglia play a large role in the on-line motor control might not be correct, and new studies suggest that the basal ganglia rather have a role in learning and habit formation (DeLong and Wichmann, 2009).

However, a combination of these two hypotheses has also been suggested (Nambu, 2008).

2.1 Anatomy of individual ganglia

The basal ganglia are divided into a dorsal and a ventral division. The dorsal division is associated with motor and associative functions, and it consists of the striatum, the globus pallidus externa and interna (GPe, GPi), the subthalamic nucleus (STN) and the substantia nigra pars reticulata and pars compacta (SNr, SNc), which will be described in detail next. The ventral division is primarily associated with limbic functions and as it is not relevant to PD, it will not be described further (Bolam et al., 2009).

2.1.1 Striatum

The striatum is divided by the internal capsule into the caudate nucleus and the putamen (Nambu, 2009).

The principal neuron of the striatum is the medium-size densely spiny neuron (MSN), see figure 2.2. The dendrites of these neurons have a short spine-free segment near the cell body, but are otherwise densely packed with spines. The neurons primarily use the neurotransmitter GABA (Bolam et al., 2009).

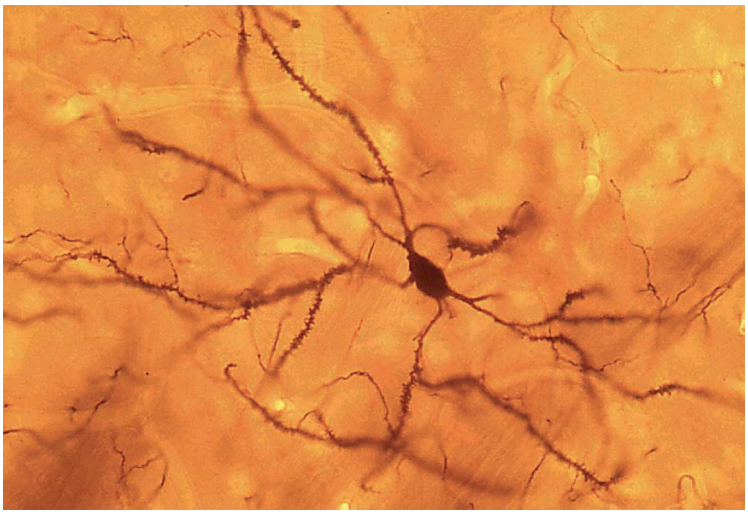

Figure 2.2: Golgi-stained Medium-size densely spiny neuron (MSN) from rat striatum. The cell body is approximately 15 μm in diameter, and four primary dendrites, each densely covered with spines, can be seen. (Bolam et al., 2009)

Input

The striatum recieves input from large parts of the cortex. The motor areas of the cortex project to the caudal part of the putamen somatotopically, and the prefrontal cortex project to the caudate nucleus and the rostral part of the putamen (Nambu, 2009).

Axons from cortical neurons make connections to the head of the spines, each cortical axon having only a few synapses with an individual MSN. However, many different cortical axons synapse on the same MSN, as these can have 10,000-15,000 spines. The spines are also

the target for input from the thalamus. Both the cell body, the neck of the spines and the dendrites themselves are targets for dopaminergic feedback from the SNc (Bolam et al., 2009; Ergun and Follett, 2007).

In addition to the MSNs, the striatum also contain GABAergic and cholinergic interneurons, which recieve input from the cortex, thalamus, GPe, SNc, and the MSNs (Bolam et al., 2009).

Output

The MSNs can be divided in two populations. One population projects to the SNr and GPi, with collaterals to the GPe, whereas the other population projects exclusively to the GPe (Bolam et al., 2009).

2.1.2 Globus pallidus externa (GPe)

The external segment of globus pallidus consists of GABAergic neurons (Bolam et al., 2009).

Input

The main input is from the striatum, but there is also input from STN and from other neurons in GPe itself (Bolam et al., 2009).

Output

In addition to their connections to the other GPe neurons, the GPe neurons project to the STN, the output nuclei of the basal ganglia, and the SNc. About a quarter of the GPe neurons innervate the striatum, connecting to the interneurons there, and through these connections the GPe can theoretically control the activity of the entire striatum (Bolam et al., 2009).

2.1.3 Subthalamic nucleus (STN)

The STN is located below the thalamus. Unlike most neurons in the basal ganglia, the neurons of the STN use the neurotransmitter glutamate, which is excitatory (Bolam et al., 2009).

Input

Large inhibitory input to the STN come from the GPe. Glutamatergic input comes from the cortex, especially the motor, pre-motor and prefrontal areas, exclusively ipsilateral and from the thalamus. The STN also receives dopaminergic input from the SNc (Bolam et al., 2009).

Output

The main outputs of the STN is to the SNr and GPi. However, neurons of the STN also innervate the GPe and the dopamine neurons of the SNc (Bolam et al., 2009).

2.1.4 Substantia nigra pars reticulata (SNr) and Globus pallidus interna (GPi)

The GPi and the SNr are the major output nuclei of the basal ganglia (Bolam et al., 2009).

Input

The main input is from the MSNs of the striatum. In addition there is input from GABAergic neurons of the GPe and glutamatergic neurons of the STN (Bolam et al., 2009).

Output

The output neurons of the GPi and SNr are large and GABAergic, and project to the thalamus, from where information is passed to the cortex and subcortical structures (Bolam et al., 2009).

2.1.5 Substantia nigra pars compacta (SNc)

The SNc consists primarily of dopamine neurons (Bolam et al., 2009; Nambu, 2009).

Input

These neurons receive GABAergic input from the striatum and the GPe, and glutamatergic input from the STN (Bolam et al., 2009; Nambu, 2009).

Output

The dopamine neurons output primarily to the striatum, but also to the GPe, the STN and the frontal cortex. It has been estimated that each dopamine neuron has around 250,000-330,000 synapses with neurons in the striatum (Bolam et al., 2009; Nambu, 2009).

2.2 Motor-related pathways

Much of the input to the basal ganglia arrives from the cortex in parallel loops, where information from individual cortical areas in the frontal lobe are processed in specific and non-overlapping areas of the basal ganglia, and returned to the same frontal lope area through specific areas in the thalamus (DeLong and Wichmann, 2009, 2007).

One of the currently five identified circuits is the skeleto-motor circuit which begins and ends in the premotor cortex, the supplementary motor area and the motor cortex. The skeleto-motor circuit is subdivided into separate somatotopic pathways for, e.g., arms, legs and facial movements. (Kandel et al., 2000)

2.2.1 The direct and indirect pathways

When not excited or inhibited, the output nuclei, GPi and SNr fire tonically and with high frequencies of 40-100 Hz, inhibiting their target nuclei in the thalamus and brainstem (Bolam

et al., 2009; Kandel et al., 2000; Nambu, 2009; Surmeier et al., 2005).

Two pathways from the striatum to the GPi and SNr modulate this inhibition, see figure 2.3 The pathways are called the direct and indirect pathways and arise from two different populations of neurons in the striatum (Bolam et al., 2009; Kandel et al., 2000).

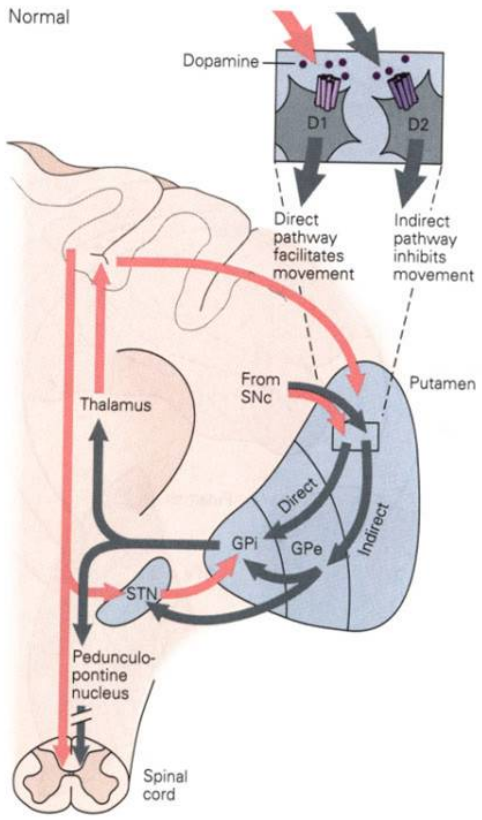

Figure 2.3: The normally functioning basal ganglia. Excitatory pathways are shown in red, and inhibitory pathways are shown in grey. Dopamine input in the putamen, which is part of the striatum, facilitates the direct pathway and inhibits the indirect pathway. (Kandel et al., 2000)

The striatal neurons in the direct pathway project monosynaptically to the SNr and GPi. The neurons express D1 dopamine receptors, and utilize GABA as neurotransmitter, having an inhibitory effect on SNr and GPi (Bolam et al., 2009; Nambu, 2009).

The striatal neurons in the indirect pathway project polysynaptically to the SNr and GPi. The neurons express D2 dopamine receptors and synapse in the GPe utilizing GABA. The next synapse is in the STN, and is also GABA-ergic. From the STN to the output nuclei glutamate, an excitatory neurotransmitter, is used. Taken together the signals from the striatum over the indirect pathway have an overall excitatory effect on the SNr and GPi, due to the two consecutive inhibitory synapses and the excitatory signal from the STN (Bolam et al., 2009; DeLong and Wichmann, 2007; Kandel et al., 2000; Nambu, 2009).

When phasic excitatory input from a part of the cortex arrives in part of the striatum, and activates the direct pathway, the targeted, tonically active, neurons in the GPi are inhibited, leading to a reduction in their firing rate. This inhibition in turn disinhibits parts of the thalamus, thereby activating parts of the cortex in the somatotopically arranged loop. On

the contrary, activating the indirect pathway leads to increased inhibition in parts of the thalamus and thereby less activation of the corresponding cortex (Bolam et al., 2009; Kandel et al., 2000).

Dopamine, released from SNc neurons projecting to the striatum, affects both the direct and indirect pathways. When dopamine interacts with the D1 dopamine receptors in the direct pathway transmission is facilitated, whereas dopamine interaction with the D2 dopamine receptors in the indirect pathway reduces transmission. However, in both pathways dopamine leads to the same overall effect, namely a reduced inhibition in the thalamus and thereby a facilitation of movements initiated in the cortex (Kandel et al., 2000).

Chapter 3

Parkinson's disease

Parkinson's disease (PD) is a progressive neurological disorder, which presents itself through a number of motor- and non-motor related features. The cardinal signs of PD are resting tremor, bradykinesia, rigidity and postural instability (Jankovic, 2008; Olanow et al., 2009).

Resting tremor is an easily recognised symptom of PD, and is also the most common symptom. However, it is estimated that 30 % of PD patients do not have resting tremor. The tremors occur at a frequency of 4-6 Hz and disappear during action and sleep (Jankovic, 2008; Olanow et al., 2009).

Bradykinesia is slowness of movement and is the most characteristic clinical feature of PD. The bradykinesia is dependent on the patient's emotional state, and excitement or external triggers can activate quick movements in a phenomenon called kinesia paradoxica. This suggests that the motor programmes of the patient are intact but difficult for the patient to access without external triggers (Jankovic, 2008).

When a limb is moved passively, rigidity shows as an increased resistance through the whole range of motion. The rigidity may lead to postural deformities especially around the neck and trunk (Jankovic, 2008).

Postural instability occurs due to loss of postural reflexes. This usually occurs after the onset of other clinical features of the disease (Jankovic, 2008).

Freezing is a form of akinesia, which is loss of movement. It is one of the most disabling symptoms of PD. However, freezing does not occur in all patients (Jankovic, 2008). Freezing most often appears as a sudden inability to move, lasting less than 10 seconds, and most commonly affects the legs while walking (Jankovic, 2008).

Postural instability and freezing of gait are the most common causes of falls in PD patients, and this increases their risk of hip fractures (Jankovic, 2008).

3.1 Etiology

5-10 % of PD patients have a pattern of inheritance in their family, and 11 different genes have been found to have a relation to the disease. However many cases do not seem to be explained by the presence of identified genes, and PD is therefore regarded as a sporadic

disorder. One of the major risk factors is age, however 10 % of patients are younger than 45 years. A variety of environmental factors have been suggested as risk factors, among these are rural living and exposure to well water, pesticides and herbicides. However, no individual toxic or environmental agent has been found to be a definite cause of PD. It has been suggested that the development of the disease requires both carrying a susceptible gene and an exposure to a specific environmental toxic (Lees et al., 2009; Olanow et al., 2009).

3.2 Pathology

The characteristic neuropathology of PD is a loss of dopamine-producing melanoneurons of the substantia nigra. The loss of these neurons result in a decreased dopaminergic tone in the motor areas of the striatum, causing increased activity in the output nuclei and thereby increased inhibition of the thalamus, see figure 3.1, leading to the bradykinesia, tremor at rest and muscle ridigity, that characterise PD (Braak and Tredici, 2008; DeLong and Wichmann, 2007; Kandel et al., 2000; Wolters, 2008).

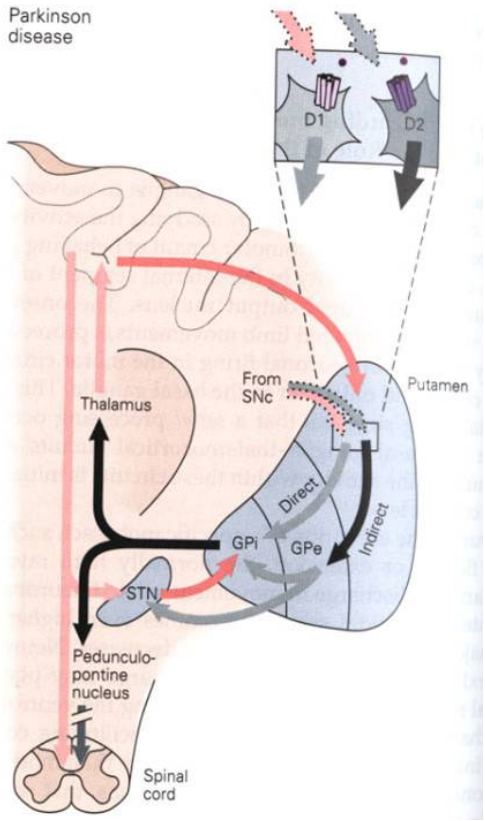

Figure 3.1: The function of the basal ganglia in Parkinson's disease. Black arrows show stronger inhibition, and faint pink arrows show weaker excitation when compared to the normal situation in figure 2.3. The reduced amount of dopamine in the putamen leads to an increased inhibition of the thalamus, through a decrease in the direct and indirect pathways' inhibition of the globus pallidus interna, which is responcible for inhibiting the thalamus. (Kandel et al., 2000)

3.2.1 Pathology of basal ganglia

Injecting certain experimental animals, particularly mice and non-human primates, with the drug 1-methyl-4-phenyl-1,2,3,6-tetrahydropyridine (MPTP), causes the animals to develop parkinson-like motor symptoms, since MPTP has a neurotoxic effect on dopaminergic neurons. This animal model has helped to understand the changes that occur in the motor circuits in PD (DeLong and Wichmann, 2007; Soderstrom et al., 2009).

In particular, the MPTP model showns an increase in tonic activity in the STN, GPi and SNr, and a decrease in GPe. This suggests that dopamine depletion leads to an increased activity in the indirect pathway, which involves an increased inhibition of GPe, leading to increased disinhibition of STN, which in turn causes an increased excitation of GPi and SNr. At the same time, the lack of dopamine leads to decreased activity in the direct pathway. Together this results in an increase in inhibitory output from the GPi and SNr leading to decreased activity in the thalamus and its cortical projections. This in turn causes slowness of movement, which is one of the main features of PD (DeLong and Wichmann, 2007; Kandel et al., 2000).

When a lesion is created in the STN in MPTP monkeys, the parkinson-like motor symptoms improve, suggesting that the excessive activity in the STN is an important factor in the creation of the slow movement characterising PD (Kandel et al., 2000).

Measurements of dopamine levels in the striatum of PD patients, and measurements of the metabolic activity throughout the basal ganglia are consistent with the disease model originally formulated based on the MPTP monkeys (Kandel et al., 2000).

However, it has been found that phasic activity also changes in the MPTP monkeys, and these changes in firing patterns might play a larger role than the changes in discharge rate. Findings suggest that the characteristic tremor associated with PD might be due to increased synchronisation of oscillatory discharges in the basal ganglia. Under normal conditions neurons in the basal ganglia rarely fire in synchrony (DeLong and Wichmann, 2007; Kandel et al., 2000).

Comparing monkeys before and after the injection of MPTP showed an increase in correlated activity, and an appearance of oscillatory activity (Lozano et al., 2010). Oscillations, particularly in the β-range of frequencies, have also been found in the basal ganglia of PD patients, and have been identified in single neurons in the GPi, SNr and STN. Oscillations in the local field potentials in the STN, GPi and cortex, had frequencies of 10-25 Hz in unmedicated patients, but the frequencies changed to 60-80 Hz when the patients were treated with levodopa or STN stimulation (DeLong and Wichmann, 2007).

3.2.2 Other neuropathological aspects

A characteristic neuropathological finding in autopsies of PD patients are Lewy bodies, which are aggregations of proteins, particularly α-synuclein, inside neurons. New theories suggest, that during the development of PD, the Lewy bodies develop in specific types of neurons throughout the entire nervous system. Studies based on autopsies of PD patients in varying stages of the disease show that the Lewy bodies do not develop simultanously throughout the nervous system. Rather, studies indicate that one of the initial sites for

Lewy body development is the anterior olfactory structures (Braak and Tredici, 2008).

At later stages of the disease, the Lewy bodies appear in specific areas of the basal portions of the mid- and forebrain. Among these areas is the substantia nigra pars compacta, where the Lewy bodies might play a role in the loss of dopamine-producing neurons (Braak and Tredici, 2008).

Progressive neural degeneration in other parts of the central and peripheral nervous system lead to the non-motor symptoms, that are also often seen in PD. Among these symptoms are: depression, anxiety, autonomic dysfunction, sleep disorders and cognitive impairment (DeLong and Wichmann, 2007; Olanow et al., 2009).

3.3 Diagnosis

The diagnosis of PD is based on observation of the cardinal signs of the disease, with at least two of the three features tremor, rigidity and bradykinesia present. A finding of degenerated dopaminergic neurons in the substantia nigra, and the presence of Lewy bodies upon autopsy confirm the diagnosis (Jankovic, 2008; Olanow et al., 2009).

New studies suggest that constipation, REM sleep behaviour disorder and anosmia, the lack of ability to perceive odours, might be early signs of PD (Olanow et al., 2009).

3.4 Treatment

Although recent findings suggest that PD involves more neuropathological aspects than just the loss of dopamine in the striatum, the primary treatment options still focus on treating the motor symptoms, that the dopamine loss cause. This section therefore only describes treatments aimed at this target.

3.4.1 Pharmacological treatment

Many different types of drugs are used in the treatment of PD patients, but the primary drug remains levodopa.

Levodopa

Dopamine cannot penetrate the blood-brain barrier, however its immediate precursor levodopa, can. Once inside the brain levodopa is then converted to dopamine by enzymes inside the nigrostriatal neurons. Levodopa is therefore used to treat the symptoms of PD, and it is currently the most effective at that (Factor and Weiner, 2007b; Olanow et al., 2009).

However, in many cases chronic use of levodopa introduces motor complications. These motor complications can be divided into two subgroups: motor fluctuations and dyskinesia (Olanow et al., 2009).

Motor fluctuations are fluctuations in the effectiveness of the medication, leading to 'on' periods where the medication works well in alleviating the symptoms, and 'off' periods where the medication does not alleviate the symptoms well (Olanow et al., 2009).

Dyskinesias are involuntary movements. When a patient has been treated with levodopa for a long time, it might be difficult to find a dose of levodopa, that alleviates the parkinson symptoms without inducing dyskinesia (Olanow et al., 2009).

New studies suggest that motor complications are caused by levodopa being delivered to the brain intermittently. This results in the striatum experiencing large differences in the amount of dopamine present. This situation is different from normal physiological conditions, where some dopamine neurons fire constantly, so the striatum has a near constant amount of dopamine present. These findings have led to experimentation with continuous infusion of levodopa or dopamine agonists, and studies have shown a reduced frequency of motor complications with this method (Olanow et al., 2009).

Dopamine agonists

In constrast to levodopa, a dopamine agonist act directly on striatal dopamine receptors, without the need for metabolic conversion in the nigrostriatal neurons, which are degenerating. Different dopamine agonists target different dopamine receptors, but it is still unclear how this may be used therapeutically. Patients treated with dopamine agonists show fewer motor fluctuations and dyskinesias compared with levodopa. However, in many cases it becomes necessary after a while to treat the patient with levodopa to maintain symptom relief (Factor and Weiner, 2007c; Lees et al., 2009; Olanow et al., 2009).

3.4.2 Surgical treatment

Motor complications that do not respond well to medical treatment are the main reason for surgical treatment(Olanow et al., 2009).

Studies of both physiology and metabolism indicate that neurons in two areas of the basal ganglia, the globus pallidus interna (GPi) and the subthalamic nucleus (STN) are more active in PD patients. Both ablation and high frequency stimulation in these areas have been shown to reduce PD symptoms, and well as a reduction in dyskinesia (Olanow et al., 2009).

Ablation

With ablation, lesions are caused in the brain tissue, using, e.g., chemical or thermal methods, and the overactive areas in the brain are thereby destroyed. However ablation carries a risk of inducing damage in neighbouring structures, which can lead to additional neurological deficits (Olanow et al., 2009).

Lesions in the GPi can only be made unilaterally, as bilateral lesions in many cases have lead to dysarthria. The unilateral lesion leads to a significant reduction in symptoms on the contra-lateral side of the body. Lesions in the STN can be made bilaterally, however this increases the risk of damaging neighbouring structures (DeLong and Wichmann, 2007; Olanow et al., 2009).

Ablation has been largely abandoned in favor of deep brain stimulation, as ablation is irreversible, and the same effect can be achieved with stimulation (Olanow et al., 2009).

3.4.3 Deep brain stimulation

Deep brain stimulation is now a well-established neurosurgical treatment option for PD (Thevathasan and Gregory, 2010). The best canditates for the procedure are those, whose PD symptoms respond well to levodopa, but who have developed debilitating motor complications after being treated with levodopa for a long time (Factor and Weiner, 2007a).

During surgery, a DBS lead is placed in either GPi or STN. A neurostimulator is implanted under the skin usually below the collar bone, and an extension wire connecting the lead and the neurostimulator is tunneled under the skin. (Lyons et al., 2003).

It is not yet known how the stimulation affects the brain to produce the observed improvements in PD symptoms (McIntyre, 2009). Chapter 4 discusses several hypothezised mechanisms.

Chapter 4

Deep brain stimulation (DBS)

The purpose of DBS is to generate extracellular electric fields in the brain tissue, which can modify pathological neural activity (McIntyre, 2009). The fields generate voltage distributions along the neural processes, and in turn the voltage distributions generate transmembrane current flow (McIntyre, 2009).

Three different classes of neurons may be affected by the stimulation: Local cells, which have their cell bodies close to the stimulation electrode; afferent inputs, which are those neurons whose axon terminals make synaptic connections with the local cells; and fibers of passage, which are axons, that come close to the stimulation electrode. (McIntyre, 2009)

The extracellular stimulation may either activate or suppress a given neuron. This depends among other things on the neuron's position with respect to the stimulation electrode and the stimulation parameters used. Different stimulation parameters can affect how much of each of the three classes of neurons, and which kind of neural elements are affected. One of the stimulation parameters is the width of the stimulation pulse, where short pulses primarily affect the axons, and longer pulses also affect the soma. (Kern and Kumar, 2007; McIntyre, 2009)

4.1 Commonly used stimulation paradigms in DBS

The most frequently used electrodes, from Medtronic, have four contacts, each 1.5 mm long and separated by gaps of either 0.5 mm for placement in the STN and GPi or 1.5 mm for placement in the GPi and thalamus (Limousin and Martinez-Torres, 2008).

The effect of DBS depends highly on the frequency used. Frequencies between 100-130 Hz have been found to provide the most clinical efficacy (Ergun and Follett, 2007; Kern and Kumar, 2007).

Table 4.1 shows typical stimulation parameters, and tabel 4.2 show parameters after long-term followup.

,

Table 4.1: Typical stimulation parameters in patients

	(Factor and Weiner, 2007a)		(Benabid et al., 2009)
Location	STN	GPi	STN
Amplitude	2.0-3.6 V	2.5-3.6 V	2.9±0.6 V
Pulse width	60-90 μs	90-120 μs	63±7.7 μs
Rate	130-185 Hz	130-185 Hz	139±18 Hz
Electrode configuration	Monopolar/bipolar	Monopolar/bipolar	Monopolar

Table 4.2: Stimulation parameters at Long-Term Follow-Up (3-4 years) (Ergun and Follett, 2007)

Location	STN	GPi
Amplitude	3.1 ± 0.5 V	3.2 ± 0.4 V
Pulse width	72 ± 20 μs	115 ± 54 μs
Rate	151 ± 23 Hz	163 ± 25 Hz
Electrode configuration	80 % monopolar	70 % monopolar

4.2 Theories on how DBS works

The exact mechanism of how DBS influences the brain activity is not yet known. The intuitive answer would be that stimulation of cell bodies or axons lead to activation and thereby the release of neurotransmitters. However, DBS has effects that are very similar to ablation of the same tissue, which entails abolishment of activation and neurotransmitter release. There are currently several general hypotheses to explain how DBS works. The answer might, however, involve more than one mechanism, and possibly all of the proposed mechanisms to some extent (Factor and Weiner, 2007a; McIntyre, 2009)

One hypothesis is that the DBS current disrupts the voltage-gated ion channels involved in membrane depolarization, thereby preventing the generation of action potentials in the cells near the electrode. The suppression of action potentials would block abnormal activity coming from the neurons, (McIntyre, 2009; Modolo and Beuter, 2009) .

A second hypothesis is that DBS current activates axon terminals making synaptic connections with the local cells, thereby producing inhibition (McIntyre, 2009).

A third hypothesis is that the DBS train depletes neurotransmitters, thereby causing synaptic transmissions to fail. The synaptic failure induced a functional inhibition on the post-synaptic neuron (Factor and Weiner, 2007a; McIntyre, 2009; Modolo and Beuter, 2009).

A fourth hypothesis is that DBS currents disrupts pathological firing patterns in the STN. The disruption of the pathological patterns means that the targets of the STN neurons in GPi can regain normal activity, which further influences the activity of thalamus and cortex (Factor and Weiner, 2007a; McIntyre, 2009; Modolo and Beuter, 2009) .

A fifth hypothesis is that DBS activates cortical fibers projecting to the STN, and antidromic spikes from the axon to the soma of the cortical neurons might collide with orthodromic spikes annihilating both. This would decrease cortical input to STN, which might be a contributing factor in the generation of pathological firing patterns (Modolo and Beuter, 2009).

Chapter 5

Electrophysiology of neurons

In order to understand the mechanism of DBS, it is necessary first to understand some aspects of the electrophysiology of neurons.

5.1 Transmembrane potentials

Neurons, like all living cells, possess a transmembrane potential, which is a potential difference across the cell membrane. The potential difference exists because positive and negative charges are unequally distributed between the inside and the outside surface of the cell membrane. The unequal distribution is created partially by differences in the permiability of the membrane to different ions, partially by active transport of different ions across the membrane (Martini, 2006).

The transmembrane potential varies over time depending on the activities of the neuron. When the neuron is at rest, its transmembrane potential is called the resting potential, and for many types of neurons the resting potential is around -70 mV, with the minus sign indicating that the inside surface of the cell membrane is more negatively charged than the outside surface (Martini, 2006).

The cell membrane contain two different kinds of channels through which specific ions can enter and exit the cell. Passive channels are always open and are therefore also called leak channels. Active channels open and close in response to specific stimuli, which can be either chemical or voltage-related, or, in the case of some sensory neurons, mechanical (Martini, 2006).

When an active channel opens in response to a specific stimulus, the rate of ion movement across the cell membrane changes, and a graded potential is created. The graded potential affects only an area of the membrane surrounding the site of the stimulation. When a neurotransmitter interacts with receptors in the postsynaptic membrane, the graded potential, that develops as active channels open, is called a postsynaptic potential (Martini, 2006).

The postsynaptic potentials can be divided into excitatory postsynaptic potentials (EPSP) and inhibitory postsynaptic potentials (IPSP). An EPSP is a graded depolarization, making the inside of the neuron less negative, as a positive ion, sodium, enters the cell. An IPSP is a graded hyperpolarization, as a positive ion, potassium, leaves the cell, making the inside

more negative (Martini, 2006).

An action potential is a propagated change in transmembrane potential. Once it is initiated it affects the entire excitable membrane, which is characterized by containing voltage-regulated channels (Martini, 2006).

5.2 Extracellular medium

As the resistivity of the cell membranes is high (several $k\Omega \cdot cm^2$) compared to the resistivity of the extracellular space ($\sim 200\ \Omega \cdot cm^2$), the extracellular space can be considered independent of the intracellular space. The extracellular is filled with extracellular fluid, in which ionic currents spread, and is considered to act as a volume conductor (Logothetis, 2008; Mitzdorf, 1985).

Inductive, magnetic and propagative effects of electric signals in the extracellular space can be neglected as long as the frequencies are within the physiological range of about 0-5 kHz. The tissue impedance in the cortex has been found to be independent of frequency, meaning that it can be descriped as an ohmic resistor, with a linear relationship between voltage and current. The resistive properties of the gray matter have been found to be largely isotropic, meaning that they are the same along any direction (Logothetis, 2008).

5.3 Field potentials

The current flow through the resistance of the extracellular fluid generates gradients of potential. The potentials generated by currents produces by various neural activities add up in extracellular fluid, which acts as a volume conductor, due to the superposition principle (Logothetis, 2008; Webster, 2009).

Electrodes inserted into the extracellular fluid measure the mean extracellular potential (mEFP), which depends on the geometrical arrangement of the nearby neurons (Logothetis, 2008):

1. In an open field the neurons are organized in laminar arrays with their dendrites facing in one direction and their somas in the other. Simultaneous activation of dendrites generates strong and easily measured dipole layers.

2. In a closed field dipoles with a spherical symmetry are created. The polarity of the measurement inside the sphere depends on the location of the electrode and measurements outside the sphere are zero.

3. An open-closed field is a combination of the two previous fields. Measurements inside the sphere measure a combination of the two fields, whereas measurements outside sphere measure only the open field component. (Logothetis, 2008)

Chapter 6

Current source density analysis

Ensemble properties of neuronal tissue can be studied by recording local field potentials (LFPs). LFPs are caused by ionic currents that flow into and out of neurons through open channels in their membrane. When ions flow into the cell the active regions of the membrane are considered to act as a current sink, as seen from the extracellular space. The ions then flow inside the cell and exit through passive channels at inactive regions of the membrane. These regions are considered as current sources to the extracellular space (Logothetis, 2008; Martini, 2006; Mitzdorf, 1985).

Current source analysis is a method that can be applied to recorded LFPs to reveal the location of current sinks and sources in the extracellular space. As the sinks and sources are caused by activation of the neurons and in turn cause the LFPs, the sinks and sources can relate neural activity and recorded signals (Mitzdorf, 1985).

6.1 Theory

The relation between the microscopic currents that flow across the membranes and the macroscopic field potential can be described as a volume average of the of the microscopic currents. The volume average of the membrane currents is equivalent to the divergence of the extracellular current density $\vec{J}$:

$$\nabla \cdot \vec{J} = I_m \tag{6.1}$$

where I_m is the current source density, a scalar quantity with dimensions $\mathrm{A/m^3}$ (Mitzdorf, 1985). The current density can be related to the electric field through Ohm's law, and the electric field can be considered the gradient of a scalar potential field. This means that the current source density can be related to the measured potentials with this formula:

$$\vec{\nabla} \cdot \sigma \cdot \vec{\nabla}\phi = -I_m \tag{6.2}$$

where σ is the conductivity and ϕ is the potential. A more detailed treatment of the derivation of the formulas can be found in appendix A (Mitzdorf, 1985).

The formula can be simplified to a one-dimensional case, in which it becomes:

$$\sigma_z \cdot \frac{\partial^2 \phi}{\partial z^2} = -I_m \tag{6.3}$$

where σ_z is the conductivity in the z-direction. This simple form of the CSD method can be intuitively conceived using Ohm's law: A steeper potential gradient means a larger current flow, and changes in the potential gradient ($\frac{\partial^2 \phi}{\partial z^2}$) then means that the current flow changes. This change in current flow can only come from membrance currents entering og leaving the extracellular space (Mitzdorf, 1985).

Examples of CSD analysis are given in figures 6.1 and 6.2.

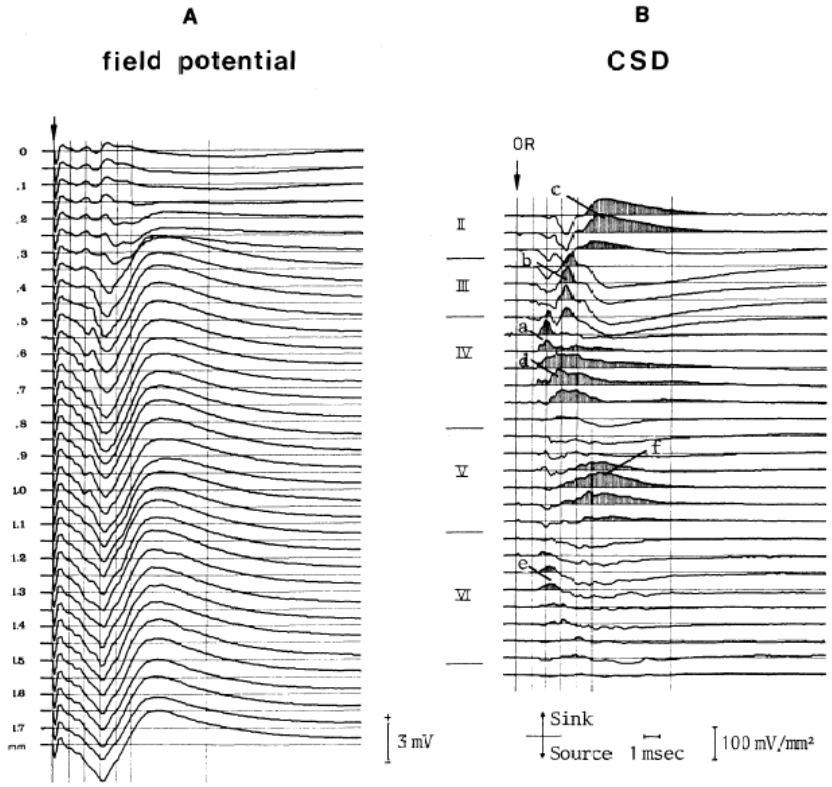

Figure 6.1: An example of CSD analysis. A: field potentials measured in the primary visual cortex of a cat. The potentials were evoked by electrical stimulation indicated by the arrow. Each trace is an average of 20 responses and the distance between recording sites were 50 μm. B: CSD calculated from the field potentials. Sinks, which correspond to active EPSP currents are shaded. Roman numerals indicate depth regions of cortex. (Mitzdorf, 1985)

In many studies using CSD analysis (e.g. Biella et al. (2002) and Mitzdorf (1985)), the field potentials are synchronized to an external stimulus and averaged. However, there are also studies (e.g. Steriade and Amzica (1996)) that use an intrinsic part of the LFP to synchronize the signals.

6.2 Interpretation

Several different kinds of neural events cause current flows across cell membranes. The activation of axons during an action potential (AP) cause a triphasic current across the

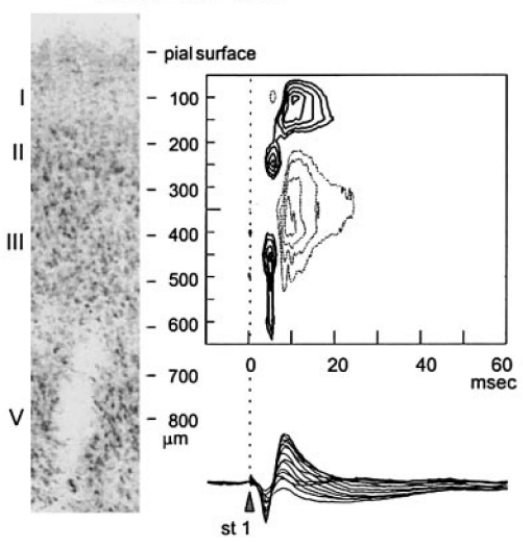

Figure 6.2: An example of CSD analysis. On the left is a coronal section showing the depth in the entorhinal cortex, which was dissected from guinea-pigs. On the right the contour plot illustrates the CSD analysis, with sinks indicated by thick lines and sources by thin lines. Below is shown the recorded field potentials at the same time scale. The arrow indicates the time of electrical stimulation. (Biella et al., 2002)

membrane, which is directed inward at the central site of activation and directed outward in front of and behind the site of activation (Mitzdorf, 1985)

When a synapse is excitatorily activated leading to an EPSP, ions flow into the cell at the activation site. An equal amount of passive capacitative and ohmic current leave the cell through the membrane at locations some distance away from the activation site. Both inward and outward currents are monophasic. If the activation of the synapse in inhibitory leading to an IPSP, there is instead an active ionic current outwards at the activation site, and inwards currents further away (Mitzdorf, 1985).

The dominant causes of CSDs are EPSPs, but IPSPs and APs may also contribute (Mitzdorf, 1985).

Chapter 7

Experimental method

7.1 Animal preparation

Animal experiments were performed by Susanne Löffler at Department for Neurology, University of Lübeck, Germany, and approved by the Ministry of agriculture, environment and rural areas of the state of Schleswig-Holstein.

Two acute experiments, referred to as 020210 and 190310 were performed on Wistar male rats weighing 480 g and 500 g respectively. The rats were initially anesthetized with isoflurane gas, and subsequently with injection of 100 μL/100g body weight Ketamine and 25 μL/ 100g body weight Rompune.

Additional doses of Ketamine and Rompune at 1/3 of the initial dose were given during the experiments as needed, approximately once an hour. Injections of glucose (1 mL, 5 %) and sodium chloride (1 mL, 0.9 %) were also given as needed.

After shaving the head of the animal, an incision was made in the skin above the skull. The location of the right subthalamic nucleus was found at +0.56 cm anterior-posterior and -0.26 cm medial-lateral in relation to the interaural point on the skull (Paxinos and Watson, 2005), see figure 7.1. A hole was drilled through the skull with a 0.9 mm drill.

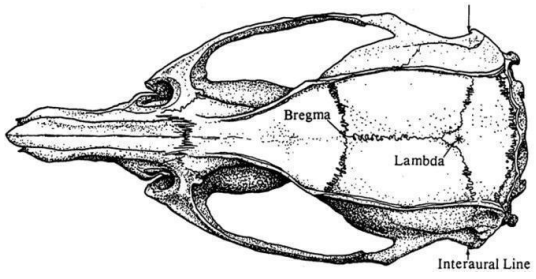

Figure 7.1: The location of bregma, lambda and the interaural line on the rat skull. The interaural point is located at where the interaural line crosses the sagittal suture. (Paxinos and Watson, 2005)

A rigid, linear array probe with seven recording electrodes (ch1-7), and one stimulation electrode (ch8) located at the tip, see figure 7.2, was used for recording. The diameter of the active sites was 70 μm, and the center-to-center distance between the recording electrodes

were 125 μm. The recording electrodes were located laterally on the probe shaft 400 μm from tip. The electrode contacts were made of gold and embedded in a stainless steel shaft with a diameter of 300 μm (Loeffler et al., 2010). The electrode was manufactured by Institut für Mikrotechnik Mainz GmbH.

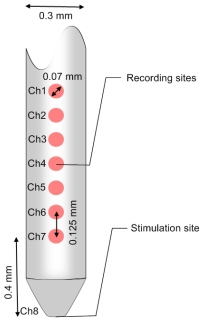

Figure 7.2: Sketch of probe with measurements and numbered recording sites. (Modified from (Loeffler et al., 2010))

The probe was inserted into the brain using a piezo drive with initial steps of 500 μm, followed by steps of 100 μm until the right subthalamic nucleus was reached at a depth of 8.5 mm in experiment 020210 and 8.6 mm in experiment 190310. Figure 7.3 shows a photograph of the experimental setup.

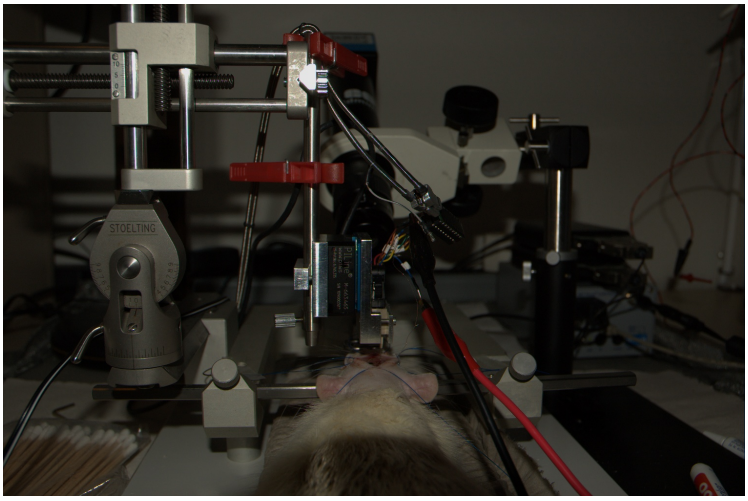

Figure 7.3: Experimental setup. The electrode is lowered into the brain of the rat by the piezo drive attached to the stereotactic device. The electrode is connected to the pre-amplifiers through the head-stage, and the black and red wire connects the electrode to the stimulator. (Löffler, 2010)

In addition a ground screw was inserted into the skull at 0.25 mm lateral and 0.25 mm anterior to the inter-aural point, and connected to ground, in addition to the electrode shaft (Loeffler et al., 2010).

7.1.1 Recording and pre-processing

The probe was connected to a ZC32 head-stage (TDT Systems, US). The analog signals were sampled with 24414.06 Hz by a Medusa pre-amplifier and passed through an optical

cable to an RZ5 BioAmp Processor (TDT Systems, US), where the continuous data were saved (Loeffler et al., 2010). The pre-amplifier has a high-pass filter with a cutoff frequency of 2.2 Hz and a low-pass filter with a cutoff frequency of 7.5 kHz (PreAmps, 2008).

7.2 Stimulation

Electrical stimulation was performed in the subthalamic nucleus using the stimulation contact electrode (number 8 on figure 7.2. A WPI A320 stimulator was used. The pulses were monophasic, cathodic and rectangular in shape.

The parameters were chosen to resemble those used in STN-DBS in clinical applications (Loeffler et al., 2010).

7.2.1 Experiment 020210

For experiment 020210 the constant stimulation parameters were a pulse width of 60 μs, a current of 0.3 mA and a frequency of 124 Hz. The varying parameter was the duration of stimulation trains, with durations of 2, 4 and 6 minutes. One minute recordings were made before and after each stimulation train, see table 7.1.

Stimulation duration	Recording duration Before	Recording duration After
2 min	1 min	1 min
4 min	1 min	1 min
6 min	1 min	1 min

Table 7.1: Stimulation and recording schedule for experiment 020210

7.2.2 Experiment 193010

For experiment 020210 the constant stimulation parameters were a pulse width of 60 μs, a frequency of 123.59 Hz and a duration of 1 minute. The varying parameter was the stimulation current, with values of 0.1-0.5 mA. Recordings of apporximate one minute were made before and after each stimulation train, see table 7.2.

Stimulation current	Recording duration Before	Recording duration After
0.1 mA	$\sim$ 1 min	$\sim$ 1 min
0.2 mA	$\sim$ 1 min	$\sim$ 1 min
0.3 mA	$\sim$ 1 min	$\sim$ 1 min
0.4 mA	$\sim$ 1 min	$\sim$ 1 min
0.5 mA	$\sim$ 1 min	$\sim$ 1 min

Table 7.2: Stimulation and recording schedule for experiment 190310

Chapter 8

Data Analysis Method

8.1 Preprocessing: Noise reduction

In many of the recordings the raw signals contained large amounts of noise at 50 Hz and additional noise at the 150, 250 350 and 450 Hz harmonics, see figure 8.1. In order to remove this noise, digital notch filters with corresponding center frequencies and a width of 1 Hz were applied to all the signals.

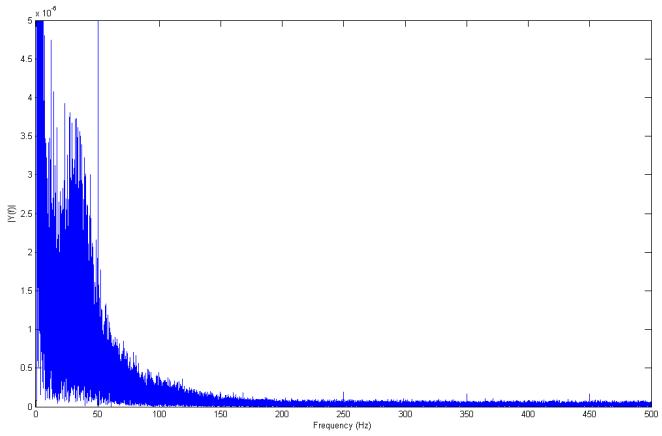

Figure 8.1: A Fourier transform of a signal shows that it contains a large amount of noise at 50 Hz plus a smaller amount at the 150, 250, 350 and 450 hz harmonics.

Some recordings also contained large amounts of energy at the dc-level, which was removed using Matlab's `detrend` function, because dc-level often reflects drift in electrodes, and it might have made it difficult to interpret the CSDs.

8.2 Preprocessing: LFP filtering

The recorded signal is a broadband signal containing frequencies from dc to $\sim$ 12 kHz. However, since it is LFPs that are the focus of the project, and, as can be seen on figure 8.2, most of the signal content is below 100 Hz, a fourth order lowpass filter with a cutoff

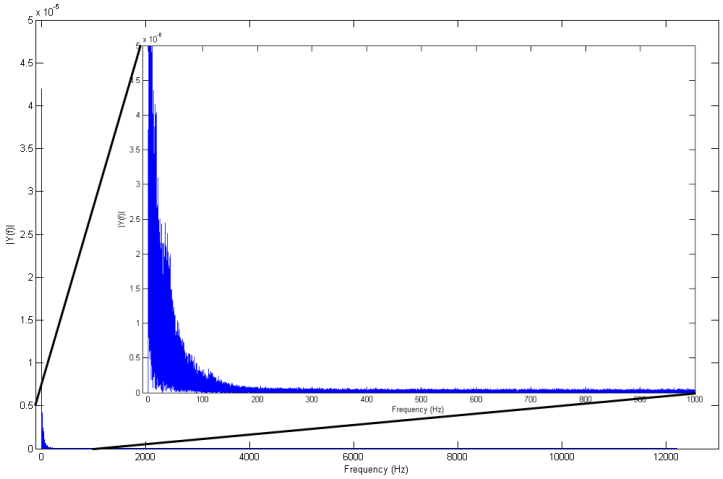

Figure 8.2: A Fourier transform of a signal after detrending and notch filters have been applied. The inset is a zoomed-in version of the same signal, showing greater detail between 0 and 1000 Hz.

frequency of 100 Hz is implemented. A butterworth filter is chosen for its maximally flat passband, so it does not change any frequencies in the LFP frequency band.

8.3 CSD calculation

Current source densities are calculated from the LFPs using the following formula;

$$Im = \frac{\phi(z + n \cdot \Delta z) - 2\phi(z) + \phi(z - n \cdot \Delta z)}{(n \cdot \Delta z)^2} \tag{8.1}$$

with ϕ being the LFP signal, $n = 1$ and $\Delta z = 1$ (Cheung et al., 2007). The conductivity is assumed to be the same in all directions, and is given a value 1, as it has not been measured. This means that the resulting CSDs are given values that are only proportional to the real values.

Experiment 190310 used seven electrodes, and CSD signals were therefore calculated at five depth. In experiment 020210, however, electrode no. 6 did not record signals, and CSD signals were therefore only calculated at three depths. Figures 8.3 and 8.4 show LFPs and corresponding CSD from experiment 020210 and 190310 respectively.

8.4 Feature extraction: RMS values of CSDs

Root mean square (RMS) is a measure of magnitude, which can be used when a signal contains both positive and negative values. In the case of CSD, RMS combines the magnitude of sources and sinks, and therefore shows the magnitude of overall activity in the local network at the specific depth.

To investigate if DBS changes the activity of the network, RMS values of the csd at each depth are calculated. The recordings before and after stimulation are compared by calculating the relative value of the after-recording compared to the before-recording.

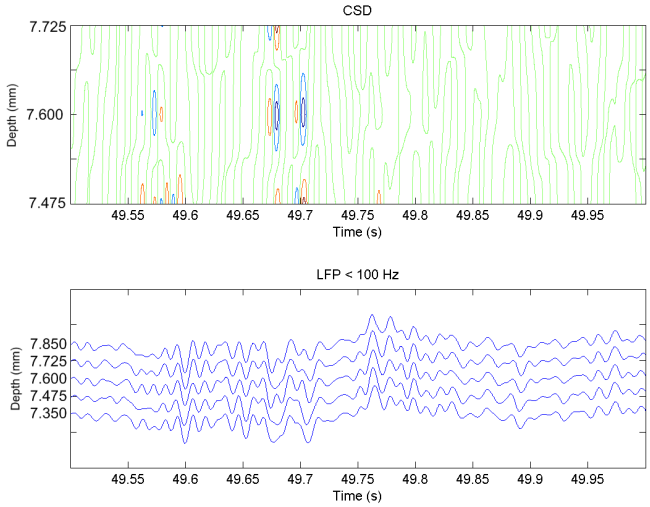

Figure 8.3: Top: CSD, bottom: corresponding LFP, from experiment 020210

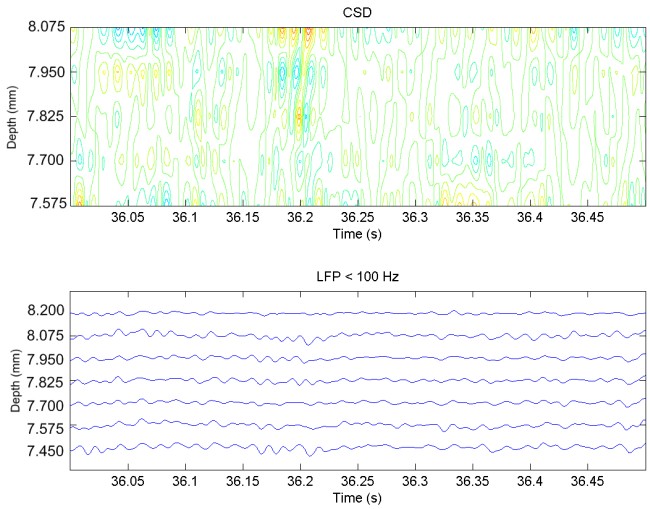

Figure 8.4: Top: CSD, bottom: corresponding LFP, from experiment 190310

8.5 Feature extraction: CSD threshold crossings

Large sinks and sources occur many times in the CSD signals, where some appear as single events and some appear as faster changes, closer together, as shown in figure 8.5.

To investigate whether these sources and sinks increase or decrease in number after DBS, they are detected and counted. Large sources were detected as ascending crossing of a threshold of 3 times the RMS value of the CSD, see figure 8.6, and large sinks as descending crossing of a threshold at minus 3 times RMS. The choice of threshold was inspired by previous work with spike detection. The number of each type of crossing was then divided by the duration of the recording. This was done for each depth individually.

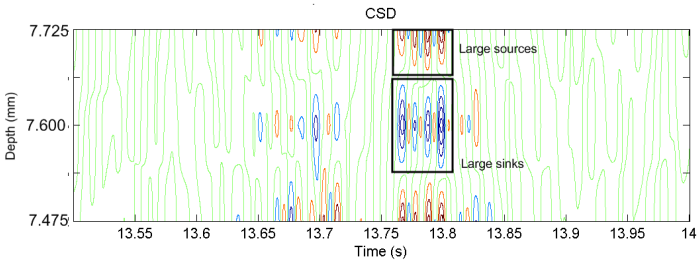

Figure 8.5: Large sinks and sources, as marked on the figure, occur many times in the CSD signals. Example from experiment 020210.

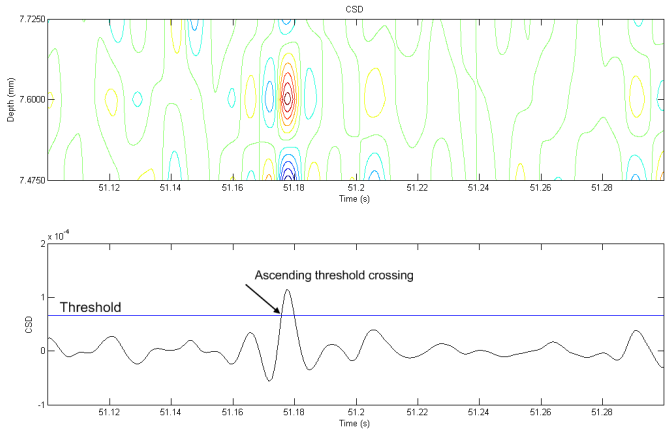

Figure 8.6: Large sources are detected by ascending threshold crossing of a threshold at 3 times RMS.

8.6 Feature extraction: Histograms of intervals between large sources

To investigate whether the timing of the large sources changes after DSB, histograms of the intervals between the detected large sources were made. The intervals were calculated as the time between a threshold crossing and the following threshold crossing. Histograms were then made based on a logarithmic time scale, in order to cover both the shortest occuring intervals, which are around 10 milliseconds, and the longest which are more than 1 second. The center intervals of each histogram bin are shown in table 8.1.

3.2 ms	4.8 ms	7.4 ms	11.3 ms	17.3 ms
26.4 ms	40.3 ms	61.6 ms	94.1 ms	143.8 ms
219.8 ms	336.0 ms	513.5 ms	784.8 ms	1.20 s
1.83 s	2.80 s	4.28 s	6.54 s	10 s

Table 8.1: Center intervals used in the making of the histograms of intervals of large sources.

Chapter 9

Results

9.1 Re-emergence of response after stimulation

Figure 9.1 shows the first 200 ms after the last stimulation pulse, for the recordings following stimulation with 0.1, 0.3. 0.4 and 0.5 mA stimulation current from experiment 190310. It was not possible to include 0.2 mA stimulation, nor to make a similar plot for experiment 020210, as data containing the time immediately after stimulation was not available in those cases.

The signals are high-pass filtered at 1000 Hz, i.e. they contain mostly spike signals.

It can be seen that the neural network was suppressed immediately following the DBS. The activity returns to the different depths of the network at different times following the end of stimulation. Higher stimulation current results in longer suppression following stimulation. Activity around electrode 5 (counted from the bottom), for example, returns after approximately 40 ms after 0.1 mA stimulation, 55 ms after 0.3 mA, 60 ms after 0.4 mA and 80 ms after 0.5 mA. The activity returns to each depth in approximately the same order regardless of stimulation amplitude, however there is not a linear relationship between the order and the distance to the stimulation electrode.

The observed suppression of the network is not likely to be due to saturation of the amplifiers, as the channels re-emerge at different times following the stimulation.

A possible explanation may be that DBS disrupts voltage-gated ion channels, as described in chapter 4, thereby preventing the membranes from depolarizing and firing. The lack of a linear relationship between the time of re-emergence and the distance to the stimulation electrode suggests that the timing may be due to anatomical differences at the different depths in the STN.

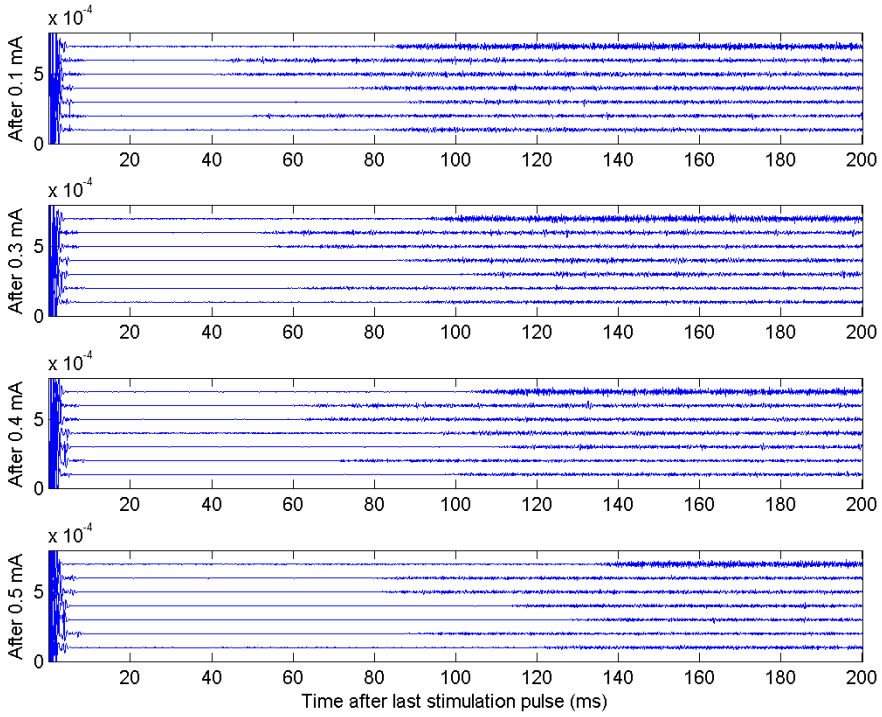

Figure 9.1: The network restarts after stimulation. The four graphs show when the network restarts after stimulation of 0.1, 0.3, 0.4 and 0.5 mA respectively. The data is from experiment 190310 and the topmost channel corresponds to the deepest electrode (at 8.2 mm), closest to the stimulation electrode, and the bottommost channel (located at 7.45 mm) was furthest from the stimulation electrode. The signals are high-pass filtered $>$ 1000 Hz, and the time is after the last stimulation pulse. It can be seen that higher stimulation current results in a longer time before the network restarts.

9.2 An interesting response to 0.5 mA stimulation

Figure 9.2 shows LFPs immediately after the last stimulation pulse to 10 s after. After the 0.5 mA stimulation, shown at the bottom of the figure, large changes in the LFP can be seen to occur on almost all channels simultaneously, beginning with intervals of approximately 0.5 seconds which then increase over time. Such large regular occuring changes are not evident after the stimulations with lower amplitude, as seen on the figure.

Figure 9.3 shows the first 60 seconds of the recording following the 0.5 mA stimulation. The large LFP changes can be seen to occur with longer and longer intervals. It is however unknown when the last change occurs as the recording is only a little more than 60 seconds long.

This finding suggests, that the network reacts differently to higher stimulation currents, and that effects of DBS can occur at least up to one minute after the stimulation has ended. However, as there is only one available recording showing the immediate effects of 0.5 mA stimulation, it is impossible to say if the observed LFP changes would always occur after 0.5 mA stimulation, or if it is a rarely occuring event. In addition it cannot entirely be ruled out that the observed changes are not caused by the 0.5 mA stimulation, but instead by some other event that took place at the same time.

If the observed LFP changes are caused by the 0.5 mA stimulation, further questions arise. One question is, whether it is desirable or undesirable that such synchronised increased activity can be caused by DBS. If the mechanism of DBS is to disrubt pathological patterns in PD patients, as described in chapter 4, it would highly undesirable if DBS caused pathological patterns of its own.

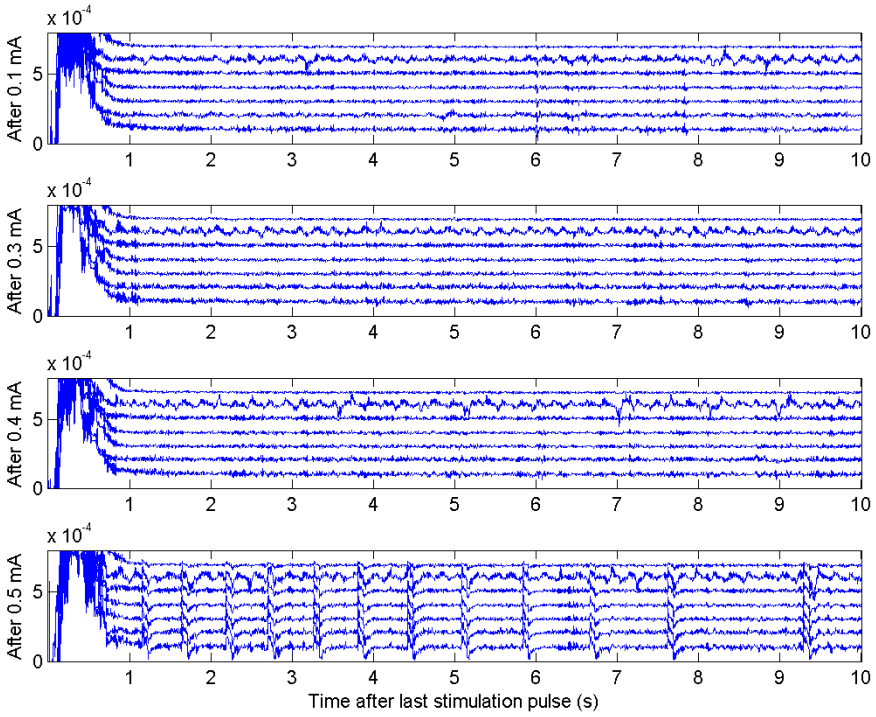

Figure 9.2: And interesting pattern appears in the LFP ($<$ 100 Hz) after stimulation with 0.5 mA. The pattern is not evident in stimulation with lower currents.

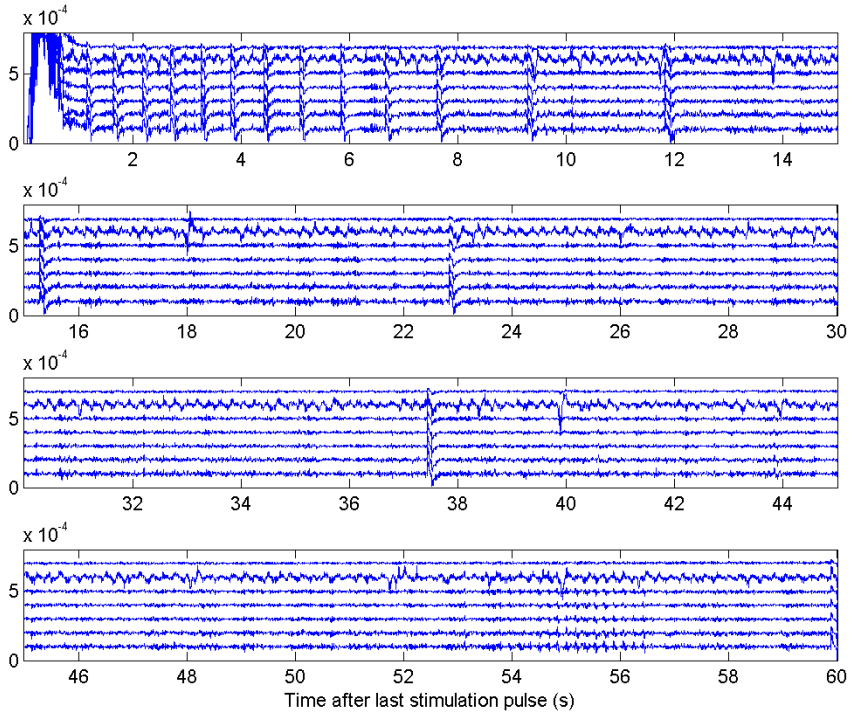

Figure 9.3: 60 seconds of the recording following the stimulation with 0.5 mA. Each panel contains 15 seconds. The pattern can be seen to occur with longer and longer intervals. The last in the recording can be seen shortly before 60 s.

9.3 RMS values of CSDs

Tables 9.1 and 9.2 show the results of calculating the RMS values of the CSD before and after DBS for experiments 020210 and 190310 respectively. The relative values show, whether the RMS has increased or decreased after the stimulation.

In experiment 020210 a slight decrease in RMS can be seen for all depth after 4 minutes of stimulation, whereas 2 and 6 minutes of stimulation produces slight increases and in some cases no change for all depths.

In experiment 190310, a decrease in RMS is seen after all stimulation currents at depths of 7.575 mm and 7.7 mm, with the largest relative decreases, 66 and 79 % respectively, occuring after the stimulation with the largest amplitude, 0.5 mA. At depth 7.825 mm almost no change is seen except for a slight increase, 108 %, after the largest amplitude. Depths 7.950 mm and 8.075 mm show almost identical patterns with a slight decrease after 0.1 mA, 92 % in both cases, almost no changes after 0.3 and 0.4 mA, and larger decreases after 0.2 and 0.5 mA, 89 % and 80 % for depth 7.950 mm, and 87 % and 78 % for depth 8.075 mm.

These findings suggest that the different locations in the STN, at the different depths of the electrode react differently to the stimulation. The deepest location at 8.075 mm is closest to the stimulation contact at the tip of the electrode, however, it is the locations farthest from the tip that experience the largest reduction in RMS of the CSD.

The findings also indicate that there is not a linear relationship between the stimulation current and the effect on the network.

Stimulation duration	RMS Before	RMS After	Relative
Depth: 7.475 mm			
2 minutes	2,3335e-05	2,4330e-05	104 %
4 minutes	2,6369e-05	2,4808e-05	94 %
6 minutes	2,4003e-05	2,3985e-05	100 %
Depth: 7.600 mm			
2 minutes	2,2315e-05	2,3193e-05	104 %
4 minutes	2,5556e-05	2,3564e-05	92 %
6 minutes	2,2145e-05	2,2742e-05	103 %
Depth: 7.725 mm			
2 minutes	1,4757e-05	1,6962e-05	115 %
4 minutes	1,8710e-05	1,8441e-05	99 %
6 minutes	1,5779e-05	1,6331e-05	103 %

Table 9.1: Relative changes in RMS of CSD before and after stimulation for each depth of experiment 020210

Apart from depth 7.825 mm, all the stimulations in experiment 190310 result in decreased or stable levels of activity, thereby supporting the hypotheses that DBS inhibits the neurons in the STN, as described in chapter 4. However, at depth 7.825, with 0.5 mA, and at depth 7.725 mm in experiment 020210 after 2 minutes stimulation with 0.3 mA, the result is increased activity, which is not explained by any of the hypotheses. However, there is not

enough data to be able to determine if the changes in activity are statistically significant.

At depths 7.950 mm and 8.075 mm in experiment 190310 a monotonous increase can be observed in the RMS values in the recordings made before each stimulation, with the values before 0.5 mA stimulation being 175 and 186 % of the values before 0.1 mA. It is not known what causes this increase in activity during the course of the experiment, it might have been an accumulating effect of stimulation, or possibly a return to normal values after the lesion caused by insertion of the electrode. However, such continuous increases in RMS value over time might have masked some of the decrease caused by DBS, causing smaller observable decreases.

Stimulation current	RMS Before	RMS After	Relative
Depth: 7.575 mm			
0.1 mA	1,5654e-05	1,2046e-05	77 %
0.2 mA	1,3509e-05	1,1707e-05	87 %
0.3 mA	1,3102e-05	1,0762e-05	82 %
0.4 mA	1,3662e-05	9,8404e-06	72 %
0.5 mA	1,8019e-05	1,1957e-05	66 %
Depth: 7.700 mm			
0.1 mA	9,0902e-06	7,5172e-06	83 %
0.2 mA	8,2348e-06	7,4741e-06	91 %
0.3 mA	7,9512e-06	6,9972e-06	88 %
0.4 mA	8,2271e-06	6,7222e-06	82 %
0.5 mA	1,0589e-05	8,3196e-06	79 %
Depth: 7.825 mm			
0.1 mA	6,6873e-06	6,5720e-06	98 %
0.2 mA	6,5890e-06	6,5884e-06	100 %
0.3 mA	6,3965e-06	6,5044e-06	102 %
0.4 mA	6,5052e-06	6,5870e-06	101 %
0.5 mA	6,7217e-06	7,2651e-06	108 %
Depth: 7.950 mm			
0.1 mA	1,3385e-05	1,2363e-05	92 %
0.2 mA	1,5142e-05	1,3459e-05	89 %
0.3 mA	1,7176e-05	1,7191e-05	100 %
0.4 mA	1,9943e-05	1,9774e-05	99 %
0.5 mA	2,3418e-05	1,8761e-05	80 %
Depth: 8.075 mm			
0.1 mA	2,5494e-05	2,3389e-05	92 %
0.2 mA	2,9861e-05	2,5997e-05	87 %
0.3 mA	3,4312e-05	3,4203e-05	100 %
0.4 mA	4,0021e-05	3,9630e-05	99 %
0.5 mA	4,7312e-05	3,6773e-05	78 %

Table 9.2: Relative changes in RMS of CSD before and after stimulation for each depth of experiment 190310()

9.4 CSD threshold crossings

Tables 9.3 and 9.4 show the number of positive and negative CSD threshold crossings per second, before and after stimulation for experiment 020210 and 190310 respectively. No clear pattern is visible for experiment 020210. The largest increase is 126 % for positive crossings, corresponding to large sources, seen after 2 minutes stimulation at depth 7.600 mm, whereas the largest decrease at 85 % is at the same depth following 4 minutes stimulation. Likewise for negative crossings, corresponding to large sinks, the largest increase at 122 % and the largest decrease at 74 % occurs at the same depth of 7.725 mm after 4 and 2 minutes stimulation respectively.

Experiment 190310 does not show a clear pattern either. No specific depth or stimulation current shows consistent in- or decrease in neither positive nor negative threshold crossings. However, 0.4 mA caused decreases (58-94 %) in both positive and negative crossings at depths 7.825 mm, 7.950 mm and 8.075 mm closest to the stimulation electrode, and 0.5 mA caused large decreases in positive crossings at depth 7.950 mm and in both positive and negative crossings at depth 8.075 mm (61-86 %). However 0.5 mA also caused increases in the number of positive crossings at depth 7.575 mm (305 %) and negative crossings at depth 7.575 mm (230 %).

Table 9.4 also shows that there are large differences in the number of threshold crossings at the different depths, where depth 7.825 mm range between 2.53 and 3.02 positive threshold crossings, and between 1.04 and 1.12 negative crossings per second before stimulation, whereas depth 7.950 mm range between 0.37 and 0.96 positive crossings and 1.03 and 1.51 negative crossings per second. This indicates that the different depths have different distributions of sources and sinks.

Stimulation duration	Positive cross/sec Before	Positive cross/sec After	Relative	Negative cross/sec Before	Negative cross/sec After	Relative
Depth: 7.475 mm						
2 minutes	2.95	2.43	116 %	2.67	3.27	122 %
4 minutes	2.92	3.60	123 %	3.27	3.27	100 %
6 minutes	3.48	3.10	89 %	2.63	2.92	111 %
Depth: 7.600 mm						
2 minutes	2.75	3.47	126 %	3.08	3.47	112 %
4 minutes	3.50	2.97	85 %	3.23	3.40	105 %
6 minutes	2.72	3.17	117 %	3.27	2.87	87 %
Depth: 7.725 mm						
2 minutes	3.20	3.75	117 %	3.00	3.65	122 %
4 minutes	3.55	3.67	103 %	3.90	2.90	74 %
6 minutes	3.50	3.55	101 %	3.13	3.08	98 %

Table 9.3: Number of crossings of threshold per second of CSD before and after stimulation at each depth for experiment 020210

As described in chapter 4, the spatial relation between a neuron and the stimulation electrode

can affect whether the neuron is activated or suppressed. This may explain how the 0.5 mA stimulation leads to fewer threshold crossings close to the stimulation electrode, while simultaneously leading to more crossings further away in experiment 190310. Different stimulation amplitudes may also have different effects, as it can be observed that the lower amplitudes, 0.1 and 0.2 mA, lead to increases in crossings closest to the stimulation electrode.

The number of threshold crossings do not correspond to neural activity in the same way as the RMS values do, as the RMS values are used in calculating the threshold. But as no previous studies of spontaneous CSD threshold crossings after DBS have been found in literature, it is difficult to say what the expected result would be.

Stimulation current	Positive cross/sec Before	Positive cross/sec After	Relative	Negative cross/sec Before	Negative cross/sec After	Relative
Depth: 7.575 mm						
0.1 mA	1.07	1.34	125 %	1.21	1.07	88 %
0.2 mA	1.37	1.25	91 %	0.79	1.11	140 %
0.3 mA	1.15	1.66	144 %	0.93	1.01	109 %
0.4 mA	0.98	1.59	162 %	0.65	1.16	178 %
0.5 mA	0.90	2.76	305 %	0.84	1.25	150 %
Depth: 7.700 mm						
0.1 mA	1.06	1.11	105 %	1.23	1.62	132 %
0.2 mA	0.88	0.92	105 %	1.55	1.59	102 %
0.3 mA	0.74	0.94	126 %	1.45	1.34	93 %
0.4 mA	0.67	0.97	146 %	1.15	1.68	146 %
0.5 mA	0.82	1.06	129 %	1.07	2.47	230 %
Depth: 7.825 mm						
0.1 mA	3.02	2,74	91 %	1.12	1.12	100 %
0.2 mA	2.68	3.03	113 %	1.10	1.39	126 %
0.3 mA	2.53	2.53	100 %	1.10	1.52	137 %
0.4 mA	2.97	2.82	94 %	1.04	0.83	80 %
0.5 mA	2.93	3.19	109 %	1.06	1.21	114 %
Depth: 7.950 mm						
0.1 mA	0.60	1.02	168 %	1.10	1.58	144 %
0.2 mA	0.43	0.65	151 %	1.25	1.37	110 %
0.3 mA	0.37	0.40	109 %	1.03	0.86	83 %
0.4 mA	0.74	0.48	65 %	1.51	1.37	90 %
0.5 mA	0.96	0.64	67 %	1.48	1.64	111 %
Depth: 8.075 mm						
0.1 mA	1.10	1.78	162 %	0.58	1.23	212 %
0.2 mA	1.03	1.09	106 %	0.26	0.58	219 %
0.3 mA	0.87	0.83	95 %	0.38	0.34	89 %
0.4 mA	1.40	1.23	88 %	0.81	0.47	58 %
0.5 mA	1.59	1.37	86 %	1.09	0.66	61 %

Table 9.4: Number of crossings of threshold per second of CSD before and after stimulation at each depth for experiment 190310

9.5 Histograms of intervals between crossings

Figures 9.4, 9.5 and 9.6 show histograms of intervals between positive threshold crossings for each depth in experiment 020210. Figures 9.7, 9.8, 9.9, 9.10 and 9.11 show the same for experiment 190310.

For experiment 020210 no clear changes occur in the distribution of intervals after stimulation. At all depths, there are many occurances of intervals around 10 ms, which indicates that many large sources occur quickly after one another. A secondary peak can in many of the histograms be seen in the bin centered around 336 ms, roughly halfway between 100 ms and 1 s.

For experiment 190310 no clear changes can be seen either. However, it is clear that there were depth-dependent differences present. Especially depth 7.825 mm stands out having many intervals around 100 ms, whereas the other depth in most cases have a large peak at 10 ms, and a smaller peak around 1 s.

Due to the 100 Hz lowpass filter it is very unlikely that two ascending threshold crossings occur with less than approximately 10 ms in between. This partially explains the large numbers of intervals around 10 ms, which also suggest that frequency content above 100 Hz might have been relevant to look at.

At the other end of the scale peaks around 1 s for experiment 190310 and around 300 ms for experiment 020210 suggest rhythmic occurances of large sources with frequencies of around 1-3 Hz. It is however unknown what may have caused such activity.

DBS stimulation does not seem to have a consistent effect on the distribution of intervals, but the small amount of data, only one recording per stimulation duration and stimulation current, makes it difficult to detect more complicated effects.

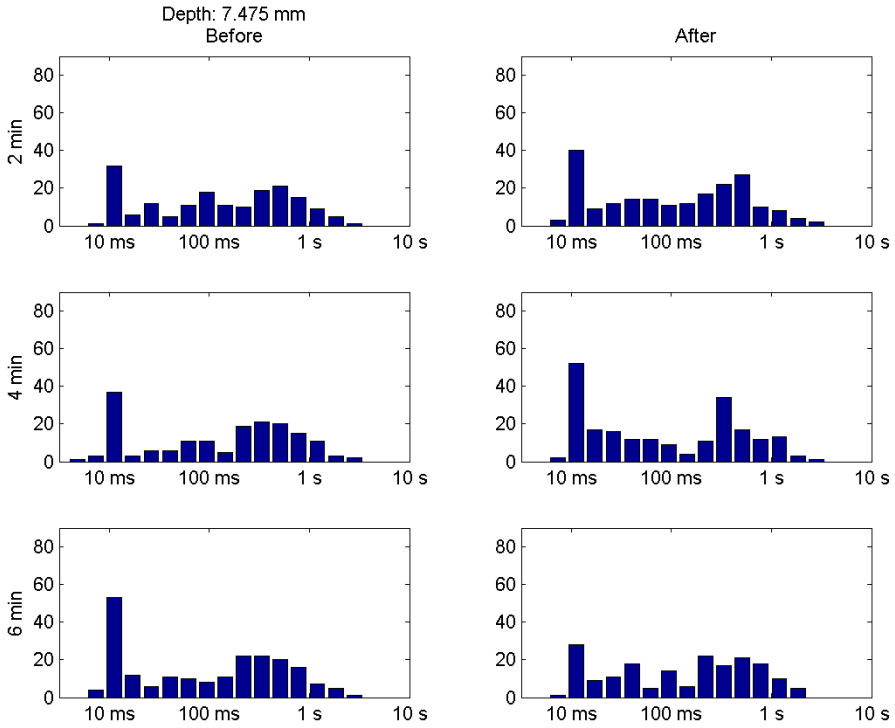

Figure 9.4: Histograms of intervals between positive threshold crossings, experiment 020210, depth 7.475 mm

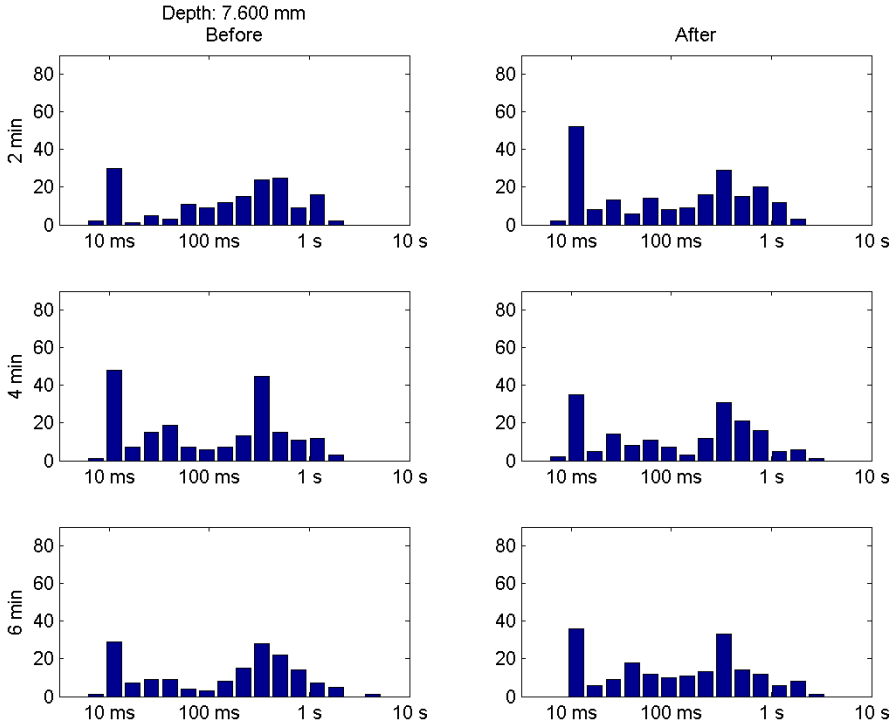

Figure 9.5: Histograms of intervals between positive threshold crossings, experiment 020210, depth 7.600 mm

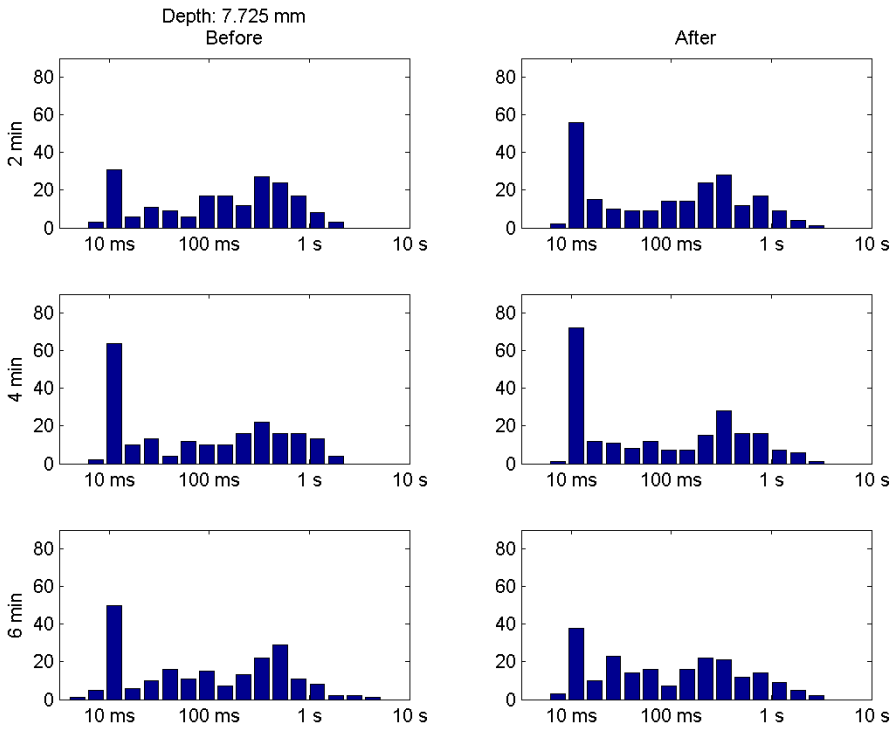

Figure 9.6: Histograms of intervals between positive threshold crossings, experiment 020210, depth 7.725 mm

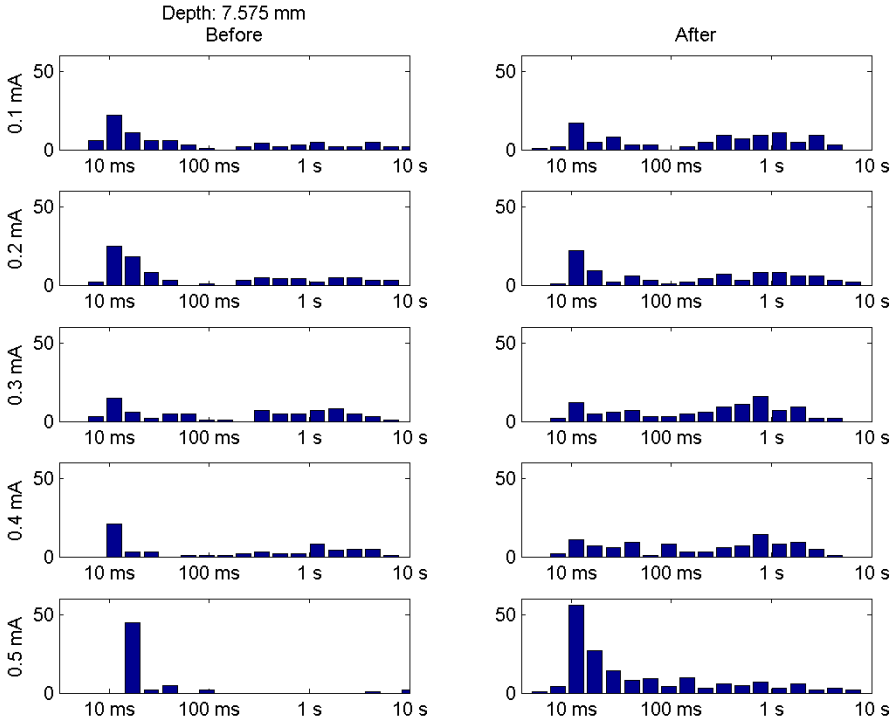

Figure 9.7: Histograms of intervals between positive threshold crossings, experiment 190310, depth 7.575 mm

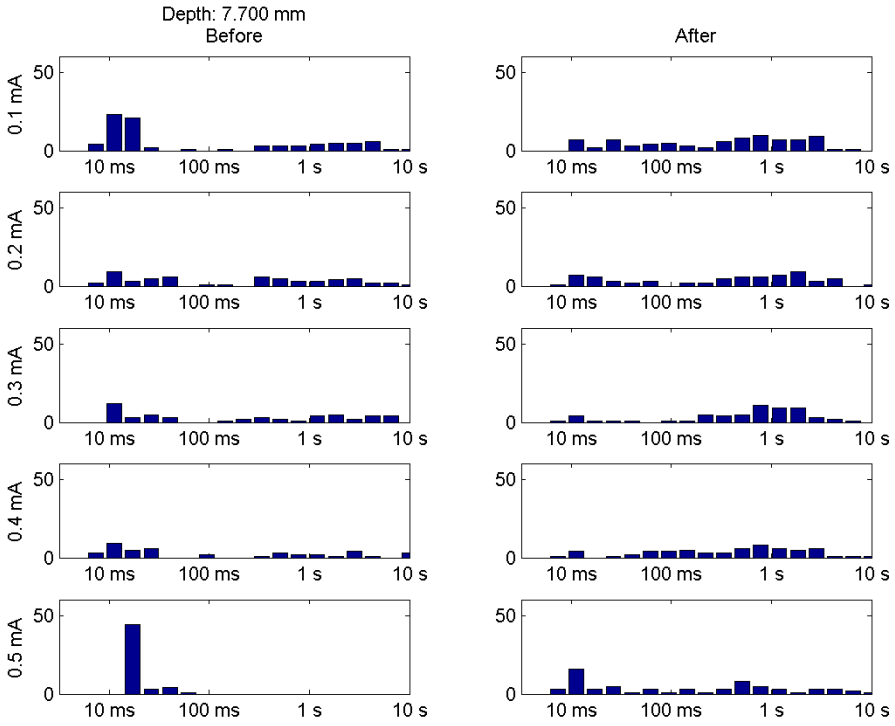

Figure 9.8: Histograms of intervals between positive threshold crossings, experiment 190310, depth 7.700 mm

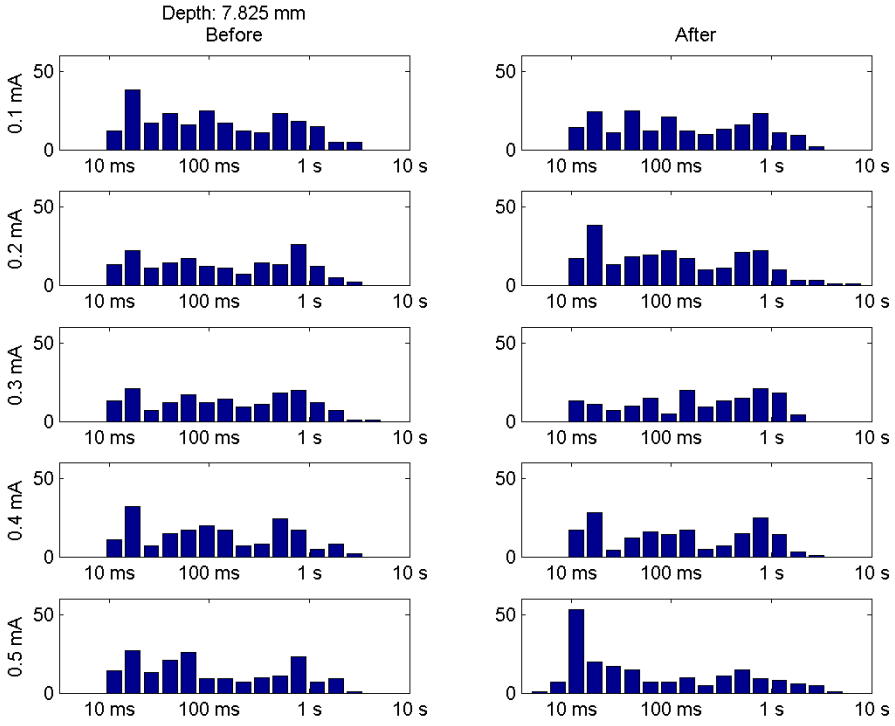

Figure 9.9: Histograms of intervals between positive threshold crossings, experiment 190310, depth 7.825 mm

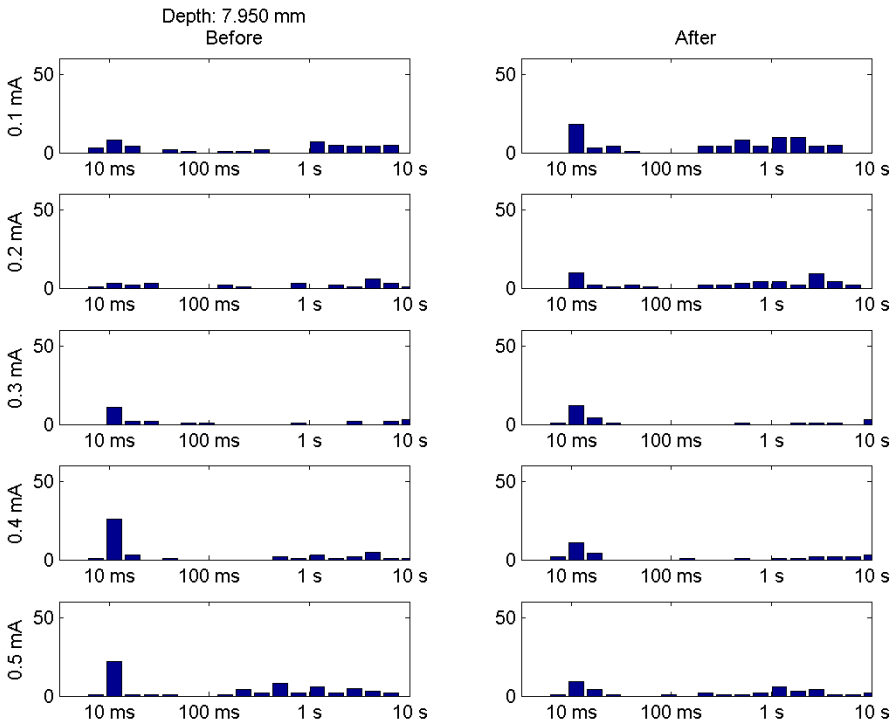

Figure 9.10: Histograms of intervals between positive threshold crossings, experiment 190310, depth 7.950 mm

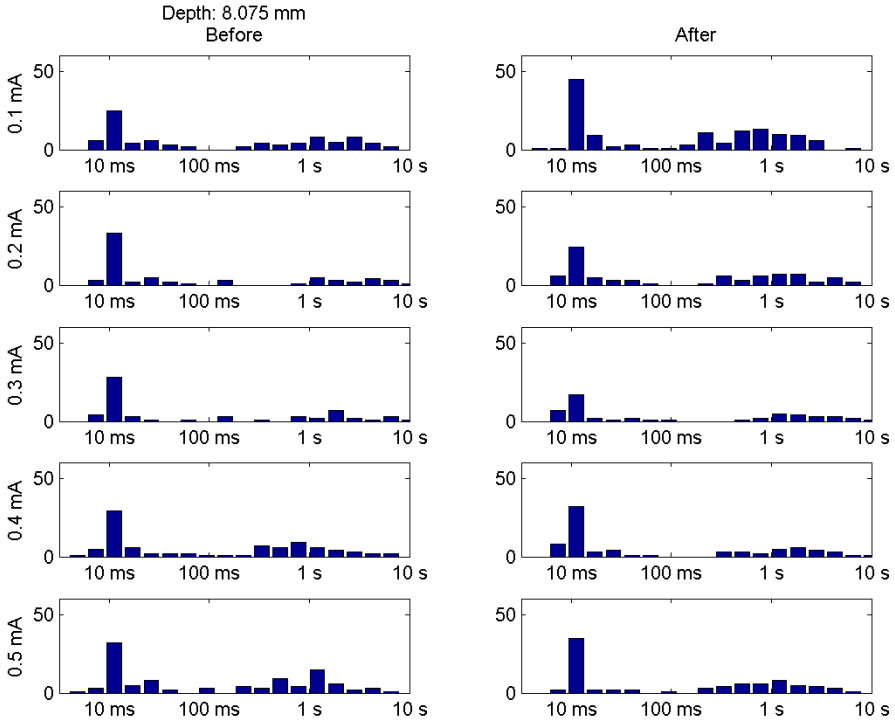

Figure 9.11: Histograms of intervals between positive threshold crossings, experiment 190310, depth 8.075 mm

Chapter 10

Discussion

10.1 Methodological considerations

Data were only available from two rats, one for each type of experiment. In order to be able to draw significant conclusions more data will be needed. Further, the obtained results are based on the assumption, that any effect of DBS had worn off before the next stimulation train. This, however, might not be the case, and an accumulation of effects from the previous stimulations might have occured. The 0.5 mA stimulation certainly showed an effect lasting at least 60 s after stimulation, and although this was the last stimulation, and no similar effect was evident from the previous stimulations with smaller amplitudes, accumulating effects cannot be entirely ruled out. When performing further experiments it would be a good idea to randomize the stimulation sequence i.e. the stimulation duration or amplitude, to be able to separate the effects of increasing parameter values from any accumulating effects.

The experiments were conducted on healthy rats, not an animal model of PD. This means that the project cannot answer any questions on how DBS affects pathological activity in the STN, only how it might affect normal activity. A larger effect of DBS on pathological activity than normal activity may be expected. In the pathology of PD, described in chapter 3 the lack of dopamine in the striatum leads to increased activity in the STN, in turn leading to greater inhibition of the thalamus, and thereby slowness of movement. Many of the theories on how DBS works presented in chapter 4 suggest that DBS has an inhibitory effect on the STN. However, this effect may not be as clear in a healthy rat where the STN is already inhibited by the rat equivalent of the GPe. Experiments similar to the ones used in this project are currently being conducted on rat Parkinson models at University of Lübeck.

No LFPs could be recorded during the actual stimulation due to large stimulation artefacts. This means that it could not be investigated what happened in the network during the stimulation, only what happened afterwards. However, it is a limitation that may be difficult to overcome, as the stimulation frequency is very high and the stimulation is provided by the same electrode array as the recording.

As no LFPs could be recorded between the stimulation artefacts, the stimulation itself could not be used for synchronization, nor were any other external synchronization stimuli

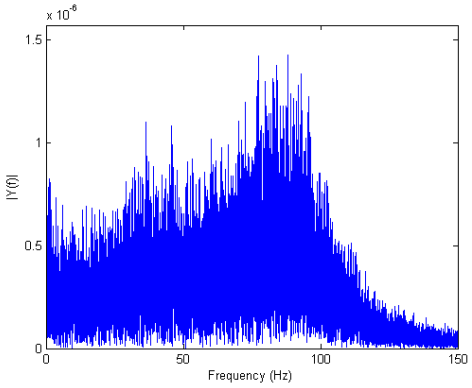

Figure 10.1: A Fourier transform of a CSD signal, showing relatively more frequency content between 50-100 Hz than between 0-50 Hz, compared to the LFP signal shown in figure 8.2 on page 28

available. In addition, no intrinsic part of the signals presented themselves as obvious to synchronize to. It was therefore necessary to use the CSD analysis to interpret spontaneous, unsynchronized activity, which has not been described as much in literature. This meant that the CSD data could not be averaged and presented as simple contour plots as in the example in figure 6.2 on page 21. For future experiments, an idea might be to use an external stimulus to elicit a repeatable response and then compare averages of this response before and after DBS.

Based on visual inspection of Fourier transform plots, it was decided to lowpass-filter the LFPs at 100 Hz. However, Fourier transforms of the CSD signals, as seen on figure 10.1, show that the CSDs contain relatively larger amounts of frequency content between 50-100 Hz, than between 0-50 Hz. One possible reason for this could be that the very low frequency contents of the LFPs represent signals originating at sites far away from the electrode, and having been lowpass filtered by the volume conduction, whereas the contents at higher frequencies represent signals with a closer origin. The calculation of the CSDs emphasizes signals of local origin, which might explain the relatively higher frequency content. In this light, it may be a good idea to have a larger cutoff frequency in the filter, as there may be relevant information above 100 Hz.

As previously mentioned, the inability to synchronize the LFPs meant that traditional methods of analysing and interpreting CSDs could not be applied. Instead, other ways of comparing the CSDs before and after DBS had to be found. This involved extracting different features from the CSD signals. The first of these features were RMS values of the CSDs calculated at each depth, with the aim of quantifying the activity in the local neural network. The RMS values made it possible to compare the level of activity before and after stimulation. However, the RMS calculation combined sources and sinks into a single value, and it might be beneficial in future work to investigate these separately.

The next feature was the number of times that the CSD signal crossed a threshold of 3 times the RMS value. This feature was inspired by looking at contour plots of the signals over time, and seeing a regular appearance of large sinks and sources, sometimes as single events, sometimes several close together. In order to count these events it was nessecary to define them in some way, and large sources were therefore defined as those that exceeded 3

times the RMS value at that particular depth, and large sinks were defined as those crossing minus 3 times the RMS value. These definitions, however, are somewhat arbitrary and do not reflect any specific physiological differences. It would be interesting, in future works, to investigate whether specific physiological mechanisms, e.g. spike bursting, underlie the observed patterns of large regularly occuring sources and sinks.

To further investigate the regularity of the occurance of these patterns histograms were made from the time intervals between the occurances. The histograms were inspired by histograms of inter-spike intervals, and clearly visualized that in addition to the many short intervals representing closely occuring events, there were many also many longer intervals representing a slower pattern of occurances. However, the histograms were difficult to compare to each other, to investigate whether DBS affected the distribution of intervals, because each histogram contained a different number of intervals. It might have been a good idea to normalize the histograms before comparing them. It may also be interesting to extract a single quantitative feature from the intervals, e.g. the mean interval length, to make comparison easier.

10.2 Depth dependency

Many of the results show that the depth is important: The re-emergence of activity happens at different times depending on depth, although always in the same order, the RMS values of CSD show different amount of decrease depending on the depth, the number of threshold crossings are different at different depth even before stimulation, and the histograms of the intervals also show differences at different depths, where especially depth 7.825 mm in experiment 190310 has a markedly different distribution than the other depths.

There are three different aspects that might have had an influence on the depth dependent results: The distance to the stimulation electrode, which might not have a linear effect; differences in the anatomy at the different depths in the STN; or differences in the electrodes or further along the signal pathway.

The timing of the re-emergence clearly depends on the stimulation current, but the order does not, nor does it depend linearly on the distance to the stimulation electrode. If different stimulation currents combined with different distances produces different results as suggested by the changes in number of threshold crossings, then that suggests that the constant order of re-emergence does not depend on the distance to the stimulation electrode, but instead on differenced in anatomy or possibly in the recording equipment. The differences in the number of threshold crossings at depth 7.825 mm compared to the other depths in experiment 190310, and the different distribution of intervals at the same depth, also before stimulation, likewise suggest an anatomical or possibly equipment related influence.

10.3 Use of CSD analysis to characterize and quantify changes in the functioning of the neural network

The re-emergence of response af stimulation clearly show an effect on a time-scale of around 100-150 ms after stimulation. The changes in LFP occuring after 0.5 mA show that effects

can occur even 60 s after stimulation. The decreasing RMS values of the CSDs also suggest that DBS does have an effect on the network after the end of stimulation. The number of threshold crossings also show changes following DBS. However, they are not as easy to interpret, nor are the histograms, which do not clearly show any change after DBS.

The use of CSD on LFP signals have revealed localized information on changes in the neural network, and suggested that both anatomy and the distance to stimulation electrode play a part in the effect of DBS. However, the lack of events to synchronize with have made it necessary to use non-traditional methods of interpreting the CSDs, and while the RMS values have shown a relatively constant decrease in activity following DBS, at least in experiment 190310, the number of threshold crossings and the intervals between them have not shown as clear changes.

Chapter 11

Conclusion

Parkinson's disease is a neurological disorder, whose classical symptoms are tremor, rigidity and slowness of movement. These symptoms are caused by degeneration of dopamine-producing neurons in the substantia nigra. Parkinson's disease is primarily treated with Levodopa, but over time this drug causes debilitating side effects, necessitating other forms of treatment. High frequency deep brain stimulation (DBS) to the subthalamic nucleus has been found to improve symptoms and in addition lessen the Levodopa-induced side effects. The purpose of DBS is to generate extracellular electric fields which can modify pathological neural activity in the basal ganglia. Many theories have been proposed to explain how this modification takes place, but no clear answer has yet been found.

Local field potentials (LFP) can give information about the functionality of the neural networks of the brain, and investigating LFP signals might provide information that could increase the understanding of how DBS functions. Using current source density (CSD) analysis on LFP signals can provide more information on local spatial relations, than the LFP signals alone, and the main hypothesis of this project has therefore been that CSD analysis can be used to characterize and quantify changes in the functioning of the neural network following DBS.

To investigate the hypothesis, data were gathered at University of Lübeck, Germany, from rat experiments where LFP signals were recorded in the subthalamic nucleus before and after DBS. Two different types of experiments were performed: one that varied the duration of stimulation and one that varied the amplitude. The data were subsequently analysed using CSD analysis, and features were extracted and used to compare the activity before and after stimulation. The features were RMS values of CSD signals at each depth, the number of times the CSD signals crossed a predetermined threshold, and the intervals between the threshold crossings.

The results showed that the RMS values of the CSD signals most often decreased after DBS. The number of threshold crossings also changed following DBS but a specific pattern was less clear. The intervals between threshold crossings showed no clear changes following DBS.

CSD analysis of LPF signals may in the future contribute more information on the effects of DBS, which may in turn lead to greater understanding of the mechanisms behind DBS, and to better treatments for Parkinson's patients.

Appendix A

Theory of current source density

This appendix gives a mathematical treatment of the theory of current source density.

The current source density, I_m, is a scalar quantity of dimension $\mathrm{A/m^3}$, and is a volume average of individual microscopic membrane currents (Mitzdorf, 1985).

A.0.1 Derivation of equation

The relation between the current source density and the measured potentials can be derived using a model of the neuronal tissue. The neuronal elements can be modelled as core conductors in cases where the length of the neuronal element is much greater than the diameter (Nicholson, 1973).

Imagine a volume V with a closed surface S, and located within the neuronal tissue. In this volume are contained m core conductors, each having a surface M_i inside S. The core conductors intersect S at n disks N_j. By subtracting these disks from S a new surface S' is created:

$$S' = S - \sum_{j=1}^{n} N_j \tag{A.1}$$

The region enclosed by $S' + \sum_{i=1}^{n} M_i$ is a closed region and contains neither sources nor sinks. The current flowing out across S' shall be called $\vec{J}$ and the current flowing out across M_i shall be called $\vec{J_m}$. Without neither sources nor sinks in the region, the net current that enters through M_i, the membranes, must also exit through S':

$$\int_{S'} \vec{J} \cdot \vec{ds} = \sum_{i=1}^{m} \int_{M_i} \vec{Jm} \cdot \vec{ds} \tag{A.2}$$

where $\vec{ds}$ is a surface element having a direction parallel to the outward normal at the center of the element (Nicholson, 1973).

An arbitrary vector field, called $\vec{P}$, and residing inside V, enclosed by S is introduced. The integral of $\vec{P}$ on S' and on the n disks, where the core conductors enter the volume then equal the surface integral over the entire surface S (Nicholson, 1973):

$$\int_{S'} \vec{P} \cdot \vec{ds} + \sum_{j=1}^{n} \int_{N_j} \vec{P} \cdot \vec{ds} = \oint_S \vec{P} \cdot \vec{ds} \tag{A.3}$$

Gauss' divergence theorem shows that the surface integral of $\vec{P}$ over the S equals the volume integral over V of the divergence of $\vec{P}$.

$$\oint_S \vec{P} \cdot \vec{ds} = \int_V \nabla \cdot \vec{P}\, d^3x \tag{A.4}$$

where d^3x is a volume element of V (Nicholson, 1973).

Defining $\vec{P}$ as being equal to $\vec{J}$ on the surface S', and equal to 0 elsewhere, then using that the surface integral of $\vec{J}$ over S' equals the surface integral of $\vec{Jm}$ over the surfaces M_i, leads to:

$$\int_V \nabla \cdot \vec{P}\, d^3x = \sum_{i=1}^{m} \int_{M_i} \vec{Jm} \cdot \vec{ds} \tag{A.5}$$

(Nicholson, 1973)

The volume current source density I_m in V is defined as a volume average of $\vec{Jm}$, leading to:

$$\int_V Im\, d^3x = \sum_{i=1}^{m} \int_{Mi} \vec{Jm} \cdot \vec{ds} \tag{A.6}$$

(Mitzdorf, 1985; Nicholson, 1973)

Using the two previous equations and the fact the V is arbitrary, leads to:

$$\nabla \cdot \vec{P} = I_m \tag{A.7}$$

(Nicholson, 1973)

As defined previously, $\vec{P} = \vec{J}$ on the boundary of S, meaning that outside the volume V, the field due to the current flowing out from V is identical for $\vec{P}$ and $\vec{J}$. However, inside V $\vec{P}$ and $\vec{J}$ are not identical. This is due to the smoothing proces and the fact that $\vec{P}$ is defined in regions of V where $\vec{J}$ is not (Nicholson, 1973).

However, as V is an arbitrary volume it can be made very small, making $\vec{P}$ and $\vec{J}$ identical in most of the tissue. The results in this equation for the current density in the tissue:

$$\nabla \cdot \vec{J} = Im \tag{A.8}$$

(Nicholson, 1973)

The extracellular medium can be considered as an ohmic resistor at physiological frequencies (Nicholson and Freeman, 1975), and the following relation then holds:

$$\vec{J} = \sigma \cdot \vec{E} \tag{A.9}$$

where $\vec{E}$ is the electric field and σ is a conductivity tensor (Mitzdorf, 1985; Nicholson, 1973).

The electric field, $\vec{E}$, is the gradient of the scalar potential field (ϕ):

$$\vec{E} = -\vec{\nabla}\phi \tag{A.10}$$

Using formulae A.9 and A.10 together leads to:

$$\vec{J} = -\sigma \cdot \vec{\nabla}\phi \tag{A.11}$$

Then inserting the equivalent of $\vec{J}$ from formula A.11 into formula A.8 gives:

$$\vec{\nabla} \cdot \sigma \cdot \vec{\nabla}\phi = -I_m \tag{A.12}$$

(Mitzdorf, 1985)

References

Benabid, A. L., Chabardes, S., Mitrofanis, J., and Pollak, P. (2009). Deep brain stimulation of the subthalamic nucleus for the treatment of parkinson's disease. *Lancet Neurol*, 8:67–81.

Biella, G., Uva, L., Hofmann, U. G., and Curtis, M. D. (2002). Associative interactions within the superficial layers of the entorhinal cortex of the guinea pig. *J Neurophysiol*, 88:1159–1165.

Bolam, J. P., Brown, M. T. C., Moss, J., , and Magill, P. J. (2009). Basal ganglia: Internal organization. In *Encyclopedia of Neuroscience*. Elsevier.

Braak, H. and Tredici, K. D. (2008). Nervous system pathology in sporadic parkinson disease. *Neurology*, 70.

Cheung, K. C., Renaud, P., Tanila, H., and Djupsund, K. (2007). Flexible polyimide microelectrode array for in vivo recordings and current source density analysis. *Biosensors and Bioelectronics*, 22:1783–1790.

DeLong, M. and Wichmann, T. (2009). Update on models of basal ganglia function and dysfunction. *Parkinsonism and Related Disorders*, 15S3:S237–S240.

DeLong, M. R. and Wichmann, T. (2007). Circuits and circuit disorders of the basal ganglia. *Arch Neurol*, 64:20–24.

Ergun, Y. and Follett, K. A. (2007). Deep brain stimulation in movement disorders. *Seminars in Neurology*, 27(2).

Factor, S. A. and Weiner, W. J. (2007a). *Parkinson's Disease: Diagnosis and Medical Management*, chapter 54. Demos Medical Publishing, 2 edition.

Factor, S. A. and Weiner, W. J. (2007b). *Parkinson's Disease: Diagnosis and Medical Management*, chapter 38. Demos Medical Publishing, 2 edition.

Factor, S. A. and Weiner, W. J. (2007c). *Parkinson's Disease: Diagnosis and Medical Management*, chapter 41. Demos Medical Publishing, 2 edition.

Jankovic, J. (2008). Parkinson's disease: clinical features and diagnosis. *J Neurol Neurosurg Psychiatry*, 79:368–376.

Kandel, E. R., Schwartz, J. H., and Jessell, T. M. (2000). *Principles of neural science*, chapter 43. McGraw-Hill, 4 edition.

Kern, D. S. and Kumar, R. (2007). Deep brain stimulation. *The Neurologist*, 13:237–252.

Lees, A. J., Hardy, J., and Revesz, T. (2009). Parkinson's disease. *Lancet*, 373:2055–66.

Löffler, S. (2010).

Limousin, P. and Martinez-Torres, I. (2008). Deep brain stimulation for parkinson's disease. *Neurotherapeutics: The Journal of the American Society for Experimental NeuroTherapeutics*, 5:309–319.

Loeffler, S., Moser, A., Wuesten, J., Detemple, P., and Hofmann, U. G. (2010). Linear array probes for microstimulation and single unit extracellular recordings in the rat's subthalamic nucleus. *Unpublished*.

Logothetis, N. K. (2008). What we can do and what we cannot do with fMRI. *Nature*, 453. SUPPLEMENTARY INFORMATION.

Lozano, A. M., Snyder, B. J., Hamani, C., Hutchison, W. D., and Dostrovsky, J. O. (2010). Basal ganglia physiology and deep brain stimulation. *Movement Disorders*, 25(Suppl. 1):S71–S75.

Lyons, K. E., Pahwa, R., and Roller, W. C. (2003). *Handbook of Parkinson's Disease*, chapter 23. Informa Healthcare.

Martini, F. H. (2006). *Fundamentals of Anatomy and Physiology*. Pearson Benjamin Cummings, 7 edition.

McIntyre, C. C. (2009). Deep brain stimulation.

Mitzdorf, U. (1985). Current source-density method and application in cat cerebral cortex: Investigation of evoked potentials and eeg phenomena. *PHYSIOLOGICAL REVIEWS*, 65(1).

Modolo, J. and Beuter, A. (2009). Linking brain dynamics, neural mechanisms, and deep brain stimulation in parkinson's disease: An integrated perspective. *Medical Engineering & Physics*, 31:615–623.

Nambu, A. (2008). Seven problems on the basal ganglia. *Current Opinion in Neurobiology*, 18:595–604.

Nambu, A. (2009). Basal ganglia: Physiological circuits. In *Encyclopedia of Neuroscience*. Elsevier.

Nicholson, C. (1973). Theoretical analysis of field potentials in anisotropic ensembles of neuronal elements. *IEEE Transactions on biomedical engineering*, BME-20(4):278–288.

Nicholson, C. and Freeman, J. A. (1975). Theory of current source-density analysis and determination of conductivity tensor for anuran cerebellum. *Journal of neurophysiology*, 38.

Olanow, C. W., Stern, M. B., and Sethi, K. (2009). The scientific and clinical basis for the treatment of parkinson disease. *Neurology*, 72 (suppl 4):S1–S136.

Parkinsonforeningen (2010). Information om parkinson. `http://www.parkinson.dk/parkinsonssygdom/informationomsygdommen/`.

Paxinos, G. and Watson, C. (2005). *The Rat Brain in Stereotaxic Coordinates*. Elsevier.

PreAmps, M. (2008). Medusa preamps. `http://www.tdt.com/products/RA16PA.htm`.

Soderstrom, K. E., Baum, G., and Kordower, J. H. (2009). Animal models of parkinsonŠs disease.

Steriade, M. and Amzica, F. (1996). Intracortical and corticothalamic coherency of fast spontaneous oscillations. *Proc. Natl. Acad. Sci. USA*, 93:2533–2538.

Surmeier, D. J., Mercer, J. N., and Chan, C. S. (2005). Autonomous pacemakers in the basal ganglia: who needs excitatory synapses anyway? *Current Opinion in Neurobiology*, 15:312–318.

Thevathasan, W. and Gregory, R. (2010). Deep brain stimulation for movement disorders. *Pract Neurol*, 10:16–26.

Webster, J. G. (2009). *Medical Instrumentation Application and Design*, chapter 4. Wiley.

Wolters, E. C. (2008). Variability in the clinical expression of parkinson's disease. *Journal of the Neurological Sciences*, 266:197–203.